

Nature Language Model: Deciphering the Language of Nature for Scientific Discovery

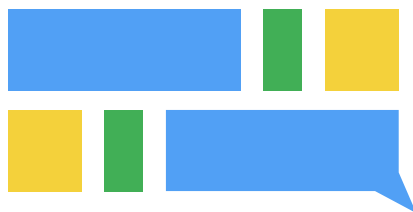
NatureLM team*
Microsoft Research AI for Science
<https://NatureLM.github.io/>

Abstract

Foundation models have revolutionized natural language processing and artificial intelligence, significantly enhancing how machines comprehend and generate human languages. Inspired by the success of these foundation models, researchers have developed foundation models for individual scientific domains, including small molecules, materials, proteins, DNA, RNA and even cells. However, these models are typically trained in isolation, lacking the ability to integrate across different scientific domains. Recognizing that entities within these domains can all be represented as sequences, which together form the “language of nature”, we introduce Nature Language Model (NatureLM), a sequence-based science foundation model designed for scientific discovery. Pre-trained with data from multiple scientific domains, NatureLM offers a unified, versatile model that enables various applications including: (i) generating and optimizing small molecules, proteins, RNA, and materials using text instructions; (ii) cross-domain generation/design, such as protein-to-molecule and protein-to-RNA generation; and (iii) top performance across different domains, matching or surpassing state-of-the-art specialist models. NatureLM offers a promising generalist approach for various scientific tasks, including drug discovery (hit generation/optimization, ADMET optimization, synthesis), novel material design, and the development of therapeutic proteins or nucleotides. We have developed NatureLM models in different sizes (1 billion, 8 billion, and 46.7 billion parameters) and observed a clear improvement in performance as the model size increases.

Keywords: Nature Language Model (NatureLM); Generative AI; Biology; Drug Discovery; Material Design

*A full list of authors is available in the Author List section on Page 59.



NatureLM

Github Repository: <https://github.com/microsoft/SFM/>

Hugging Face Repositories:

<https://huggingface.co/microsoft/NatureLM-8x7B>

<https://huggingface.co/microsoft/NatureLM-8x7B-Inst>

Contents

1	Introduction	5
2	Method	10
2.1	Pre-training data	10
2.2	Post-training data	13
2.3	Model architecture	13
2.4	Continued pre-training	14
2.5	Post-training	15
2.6	Inference acceleration	16
3	Small molecule tasks	17
3.1	Unconditional molecular generation	17
3.2	Property-to-molecule generation	18
3.3	Translation between SMILES and IUPAC	19
3.4	Target-aware hit compound generation and optimization	19
3.5	Text-guided binding affinity optimization	21
3.6	Text-guided metabolism & distributional property optimization	23
3.7	Retrosynthesis prediction	24
4	Protein tasks	27
4.1	Unconditioned generation	27
4.2	Text-guided protein generation	28
4.3	Antigen-binding CDR-H3 design	29
4.4	Protein characteristics description generation	30
4.5	Heme-binding protein design driven by text and SMILES	31
5	Material tasks	35
5.1	Unconditional material generation	35
5.2	Material generation for given composition	36
5.3	Material generation for desired properties	36
5.4	NatureLM-Mat3D: a crystal structure predictor for materials	39
6	Nucleotide tasks	42
6.1	Unconditional RNA generation	42
6.2	Guide RNA design	43
6.3	Protein binding RNA design	44
7	Prediction tasks	47
7.1	Small molecule prediction tasks	47
7.2	Protein prediction tasks	48
7.3	DNA prediction tasks	49
8	Strategies to further improve performance	50
8.1	Reinforcement enhanced NatureLM	50
8.2	Dedicated fine-tuning on retrosynthesis	51

4 CONTENTS

8.3	Dedicated fine-tuning on Matbench	52
9	Text capabilities	53
9.1	Case study	53
9.1.1	CRISPR gene editing	53
9.1.2	Cancer immunotherapy	54
9.1.3	Drug discovery	54
9.2	Comparison on AlpacaEval evaluation	55
10	Ablation study	56
10.1	Impact of text-based post-training data	56
10.2	Impact of continued pre-training on scientific data	57
11	Discussions	57
11.1	Summary	57
11.2	Limitations	57
11.3	Cross-domain applications	58
A	Supplementary figures	72
B	Supplementary tables	89
C	Supplementary notes	92
C.1	Text-guided basic property optimization of small molecule compounds	92
C.2	Supplementary information of RNA generation	93
C.3	POSCAR files of crystal structures in Fig. 17	93
C.4	Supplementary information for evaluation metrics	93
C.5	Shift the focus from general text to scientific sequences	94

1 Introduction

Foundation models, including the GPT [1–3], Gemini [4, 5], Phi [6, 7], Llama [8], Mistral [9, 10], DeepSeek [11, 12], and Qwen [13, 14], represent a transformative advancement in artificial intelligence. These models, trained on massive web-scale datasets, are designed to serve as general-purpose tools, capable of handling a wide range of tasks with a single architecture. The most notable capabilities of foundation models include their abilities to perform tasks without fine-tuning, a phenomenon known as zero-shot learning, and their few-shot learning abilities which allow them to adapt to new tasks by drawing inferences from just a few examples.

Despite their success in general-purpose tasks, early investigations [15] highlight significant room for improvement in scientific tasks involving small molecules, proteins, DNA, RNA, or materials. In particular, foundation models struggle with precise quantitative predictions (e.g., ligand-protein binding affinity, protein-protein interactions, DNA properties) [15], as well as the rational design of small molecule compounds, proteins, or materials. Ensuring the scientific accuracy of outputs from these models remains a grand challenge.

Recently, there has been a concerted effort to develop large-scale foundation models specifically tailored for scientific tasks. These approaches can be broadly divided into four categories:

1. Domain-specific foundation models. These models, such as ProGen [16] and ESM3 [17] for proteins, DNABERT [18] and Evo [19] for DNA sequences, scGPT [20] for single-cell data, and chemical language models [21, 22] for small molecules, are trained specifically on token sequence representations for individual scientific domains.
2. Fine-tuned general-purpose models. This approach adapts well-trained large language models for specific scientific domains, as demonstrated by Tx-LLM [23] for small molecules and ProLLAMA [24] for proteins.
3. Scientific data enhanced large language models (LLMs). This approach, exemplified by works such as [21, 25, 26], trains LLMs from scratch mainly with text data and a small portion of scientific data.
4. Integration of specific scientific modules. In this approach, external modules, such as pre-trained molecular or protein encoders, are integrated into general-purpose models (e.g., Llama) via lightweight adapters [27, 28].

While these approaches have made considerable progress, they do face notable limitations. Domain-specific models (approach #1) are restricted to their respective fields, limiting their ability to capture interdisciplinary insights for cross-domain applications. Fine-tuning general-purpose models (approach #2) and scientific data enhanced LLMs (approach #3) show promise but are often constrained by small-scale scientific datasets, e.g., around 90% text data and only 10% scientific data in [26], which hinders the models’ capacity to capture the complexity of scientific tasks. The integration of external modules (approach #4) faces challenges in aligning inputs effectively with large

6 CONTENTS

language models, and most implementations opt for limited fine-tuning with small datasets, leaving the core models largely unchanged.

These limitations emphasize the necessity for a science foundation model, to fulfill the sophisticated demands of scientific research. A model of this kind must not only be highly proficient in producing precise scientific predictions, but also adept at designing and optimizing scientific entities conditioned on context information. A good science foundation model ought to have the capacity to handle a diverse range of inputs. These inputs can span from literature text, to scientific sequence data such as protein or DNA sequences, and further to structural data like 3D protein/DNA structures and their dynamic behaviors. In the present study, our focus is on sequence-based data for representing biological, chemical, material systems, and textual human language (e.g., English):

- DNA, RNA, and proteins, which are often referred to as the “language of nature”, are intrinsically represented by sequences. Additionally, many other scientific entities like small molecules and materials can be effectively represented as sequences through well-established domain-specific techniques [29].
- Sequence data is highly compatible with the current mainstream large language models (LLMs). Through the continuous pre-training of LLMs, we are able to utilize the scientific knowledge embedded in these general-purpose LLMs to tackle complex scientific challenges.
- Sequential data provides remarkable flexibility when combined with autoregressive paradigms [30, 31]. These paradigms, which are extensively employed in generative models, are capable of effectively modeling the highly complex distributions of any scientific object that can be presented in the form of a sequence.

NatureLM is designed to handle the complexity of small molecules, proteins, DNA, RNA, materials, and their associated textual information. An overview of NatureLM is in Fig. 1. NatureLM follows the Transformer decoder architecture and is trained on a corpus of 143 billion tokens collected from various scientific domains (Fig. 4). Our experiments demonstrate that NatureLM significantly outperforms general-purpose foundation models for scientific tasks. Specifically, NatureLM excels in tasks such as:

1. Following textual instructions to generate and optimize scientific molecular entities.
2. Performing cross-domain generation tasks, such as designing small molecules or RNA binders for proteins as well as designing guide RNA sequences given a DNA template for CRISPR systems.
3. Achieving top performance on generation and translation tasks, such retrosynthesis (Section 3.7), SMILES-to-IUPAC translation (Section 3.3), protein generation (Section 4.1), matching or surpassing state-of-the-art specialist models.

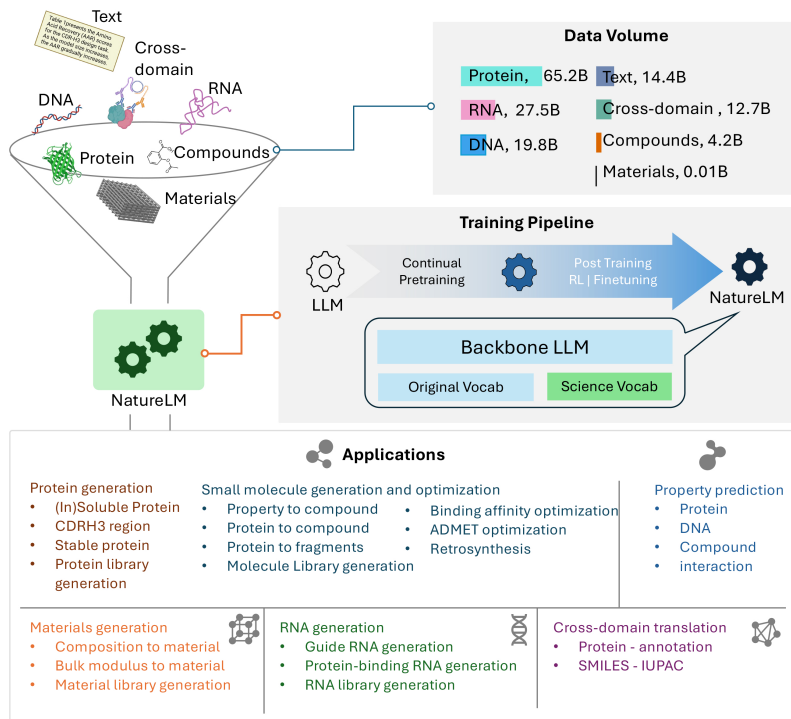


Fig. 1: NatureLM is a GPT-style generative model trained on a diverse range of data, including small molecule compounds, proteins, DNA, RNA, materials, and both general and scientific texts, amounting to a total of 143 billion tokens. It is built on existing large language models by integrating new vocabularies for scientific entities and jointly pre-training all components. After the pre-training, the model undergoes additional instruction tuning using millions of curated instructions from scientific fields. Options for reinforcement learning and dedicated fine-tuning are also available to boost performance on specific tasks. Users can engage with NatureLM through natural language inputs. The model excels in various domains, achieving top results in tasks such as retrosynthesis (Section 3.7), SMILES-to-IUPAC translation (Section 3.3), protein generation (Section 4.1) and material property prediction (Section 8.3), often matching or exceeding the capabilities of state-of-the-art specialized models.

To investigate the scalability of NatureLM with respect to model size, we trained three versions of NatureLM with varying parameter configurations. As illustrated in Fig. 2, among the 22 categories of tasks evaluated, 18 categories exhibited clear improvements with increasing model size (i.e., 8x7B demonstrated the best performance¹, followed by 8B, and then 1B), underscoring

¹The 8x7B model is a Mixture-of-Experts (MoE) model [10], composed of eight expert models, each with 7 billion parameters. A portion of these expert models is shared across all models, resulting in a total parameter count of 46.7 billion.

8 CONTENTS

the potential of large foundation models for scientific discovery. Additionally, we demonstrate the efficacy of *reinforcement learning* in enhancing the post-training performance of NatureLM for molecular property optimization and *dedicated finetuning* for retrosynthesis.

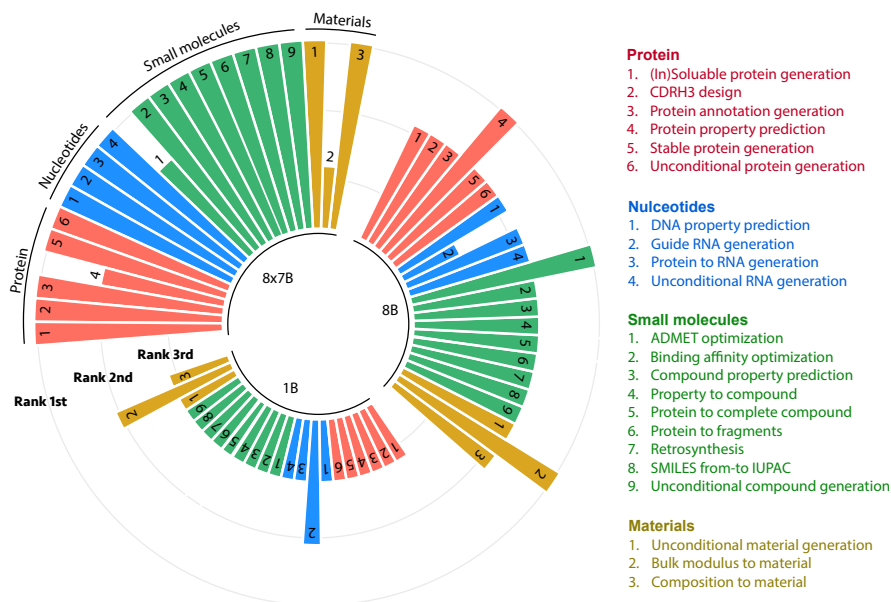


Fig. 2: The scaling effect in NatureLM is obvious. The chart depicts the overall ranking of models with varying sizes, where a better rank is represented by the “outsider” bar. The 8x7B model achieves top performance in 19 tasks, while the 8B model excels in 3 tasks. 18 categories exhibited performance improvements with increasing model size (i.e., 8x7B demonstrated the best performance, followed by 8B, and then 1B), highlighting the potential of large foundation models for scientific applications.

In summary, NatureLM represents a significant step towards building a generalist model across multiple scientific domains. By harnessing the capabilities of text-based instructions, NatureLM serves as a powerful tool for scientific discovery, enabling cross-domain generation and optimization in areas such as drug discovery, materials science, and the development of therapeutic proteins and nucleotides. Ideally, a foundation model should support a broad range of tasks while demonstrating strong zero-shot and few-shot capabilities. NatureLM shows great promise, but its language capabilities and few-shot learning skills still lag behind leading large language models. We will address

these limitations in future iterations, positioning NatureLM as an essential component in the continued evolution of science foundation models.

2 Method

2.1 Pre-training data

The pre-training data includes text, small molecules, proteins, materials, DNA, and RNA, all in the format of sequences:

1. Small molecules are converted into Simplified Molecular Input Line Entry System (SMILES) notations, obtained by applying depth-first search algorithm on molecular graphs to yield a linear representation of the chemical structure [29]. The SMILES are tokenized by the commonly used regular expression for molecules².
2. Proteins, DNA and RNA are depicted using FASTA format, which sequentially lists the amino acids or nucleotides. The sequences are tokenized into individual units, with proteins broken down into their constituent amino acids and DNA/RNA into their respective nucleotides.
3. For crystal material data, both the chemical composition and the associated space group number³ are flattened into a sequence. For example, consider the material from the material project with ID mp-1960, as shown in Fig. 3. This material has 12 atoms in its cell, consisting of 4 Li and 8 O atoms. We flatten this information as depicted in the figure. The space group is Fm3m, which corresponds to the International Space Group Number 225, and we represent it with $\langle \text{sg} \dots \rangle$.

An example of the data is in Fig. 3. The vocabulary sizes of small molecules, proteins, material, DNA and RNA are 1401, 26, 396, 16 and 16 respectively. To differentiate scientific entities from regular text, each scientific sequence is enclosed by a pair of special tokens: $\langle \text{mol} \rangle \dots \langle / \text{mol} \rangle$ for small molecules, $\langle \text{protein} \rangle \dots \langle / \text{protein} \rangle$ for proteins, $\langle \text{material} \rangle \dots \langle / \text{material} \rangle$ for materials, $\langle \text{dna} \rangle \dots \langle / \text{dna} \rangle$ for DNA and $\langle \text{rna} \rangle \dots \langle / \text{rna} \rangle$ for RNA. Specifically, we use $\langle \text{product} \rangle \dots \langle / \text{product} \rangle$ and $\langle \text{reactant} \rangle \dots \langle / \text{reactant} \rangle$ to represent products and reactants for small molecules in chemical reactions. We use $\langle \text{antibody} \rangle \dots \langle / \text{antibody} \rangle$ to denote antibodies. For example, benzene is represented by $\langle \text{mol} \rangle \text{c1ccccc1} \langle / \text{mol} \rangle$. More examples can be found within the following sections.

The pre-training data contains single-domain sequences and cross-domain sequences. A single-domain sequence comes from one domain, such as pure text sequences, SMILES sequences for small molecules, and FASTA sequences for proteins. A cross-domain sequence includes data from two different domains, building connections across domains. The distribution of our pre-training data is visualized in Fig. 4 and more details are left in Table S1.

Our cross-domain data is organized into three categories.

²https://github.com/microsoft/DVMP/blob/main/molecule/tokenize_re.py#L11

³https://en.wikipedia.org/wiki/List_of_space_groups

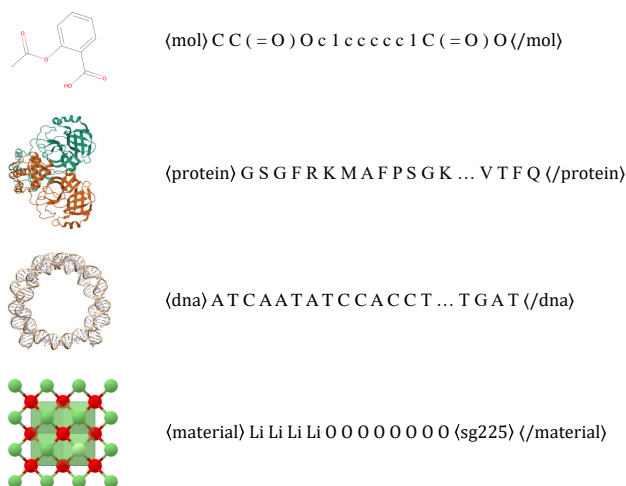


Fig. 3: Example data from each domain. The small molecule is Aspirin (PubChem CID: 2244) and visualized by RDKit [32]. The protein snapshot is from the PDB bank with ID 7CAM [33]. The DNA structure is split into chain I and chain J from PDB 1KX5 [34] and visualized by UCSF Chimera [35]. The material snapshot is from the material project with ID mp-1960 [36].

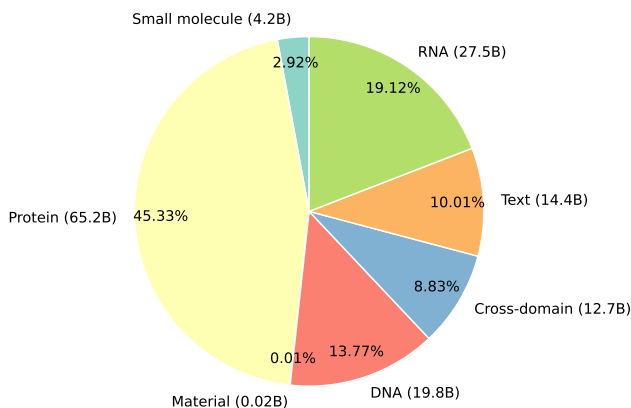


Fig. 4: Distribution of the pre-training data, measured by the number of tokens of each category.

1. Interleaved Sequences: Inspired by [21], we process scientific literature by initially employing a named entity recognition tool, BERN2 [37], to identify the mentions of small molecules and proteins within the corpus. These entities are then converted into their corresponding SMILES and FASTA

sequences. Consequently, the small molecules and proteins are wrapped by text, creating an interleaved data structure that bridges the gap between textual information and scientific data. We also develop a quality filter to remove low-quality sentences. This formulation is also similar to the one that has been used in multi-modal LLMs where image tokens are wrapped inside text [38–40]. We provide an example of interleaved sequences.

A prospective, randomized clinical trial was performed to study the efficacy of povidone iodine C=CN1CCCC1=O.II (Beta-dine C=CN1CCCC1=O.II) suppositories for the treatment of bacterial vaginosis (BV) in comparison to capsules containing lactobacilli (Dderlein Med).

2. Parallel Text and Scientific Entities: Leveraging databases such as PubChem⁴, UniProt⁵, and NCBI⁶, we extract descriptive information about specific proteins and small molecules. Additionally, from the Materials Project website⁷, material-related data such as bandgap, energy above hull, and other properties are gathered and translated into textual descriptions. This process results in parallel datasets that align scientific facts with their textual counterparts, enhancing the richness of the information.
3. Linking DNA with Proteins Through the Central Dogma: For DNA sequences, we identify segments that can be transcribed and translated into proteins, following the central dogma of molecular biology. These identified DNA segments are then replaced with the equivalent protein sequences, establishing a direct connection between the genetic blueprint and its functional protein products. This method not only reflects the biological process but also creates a dataset that encapsulates the relationship between nucleotide and amino acid sequences. We retrieved data from the RefSeq database⁸ and extracted protein sequences, including their isoforms, from annotated genes, along with their corresponding flanking DNA sequences.

	Samples (by million)	Tokens (by billion)	Samples (%)	Tokens (%)
Interleaved Sequence	4.3	4.0	10.2	31.3
Text-SMILES	33.0	3.0	78.8	24.0
Text-protein	1.9	1.4	4.6	10.8
Text-material	1.7	0.2	4.0	1.6
DNA-protein	1.0	4.1	2.4	32.3
Total	41.9	12.7	100	100

Table 1: Statistics of cross-domain data.

⁴<https://pubchem.ncbi.nlm.nih.gov/>

⁵<https://www.uniprot.org/>

⁶<https://www.ncbi.nlm.nih.gov/>

⁷<https://next-gen.materialsproject.org/>

⁸<https://www.ncbi.nlm.nih.gov/refseq/>

The statistics of cross-domain data is in Table 1. Both interleaved sequences and text-science parallel data are types of cross-domain data that aim to facilitate cross-domain connections. For interleaved sequences, the sources are literature, which covers a broader range of general topics and wider domains. In contrast, parallel data sources are existing databases that focus on specific properties. Although the topics covered by parallel data are not as diverse as those in interleaved sequences, the amount of data available for each given property is larger. These distinctions highlight the complementary nature of the two types of cross-domain data.

2.2 Post-training data

We curated a dataset for post-training with about 5.1 million instruction-response pairs encompassing six domains, small molecules, proteins, materials, DNA, RNA and general text (Figure 5). The dataset includes over 60 categories of tasks. For each task category, multiple prompts were manually crafted to form diverse instruction-response pairs, covering essential scientific tasks such as molecular optimization, antibody design, and guide RNA design. We provide two examples below:

▷ **Example 1:**

Instruction:

Create a guiding RNA to interact with the DNA sequence
`<dna>CCCAGAGC...GGGCCTGTC</dna>`.

Response:`<rna>AGGGGACAAACCTTCATCCA</rna>`

▷ **Example 2 Instruction:**

What can be produced when these reactants combine?

`<reactants>CNC.C1(=O)CCCC1Cc1c[nH]c2ccc(C#N)cc12</reactants>`

Response:

`<product>CN(C)C1CCCC1Cc1c[nH]c2ccc(C#N)cc12</product>`

The text data were sourced from open-source instruction tuning datasets like OIG⁹, aiming to ensure that the model not only excels in scientific tasks but also maintains general language capabilities.

2.3 Model architecture

NatureLM models are built upon well-trained large language models (LLMs) with some additional parameters for newly introduce scientific tokens. We used Llama 3 8B [8] and Mixtral 8x7B [10] to initialize the main part of NatureLM and continued pre-training using the science data described in Section 2.1. Additionally, we trained a model with 1B parameters, which replicates the structural design of Llama 3 but with a reduced number of layers and smaller hidden dimensions. The pre-training of NatureLM 1B begins with a random selection of 300 billion pure text tokens from the SlimPajama dataset [41], followed by the science data we collected in Section 2.1. This approach ensures

⁹<https://huggingface.co/datasets/laion/OIG>

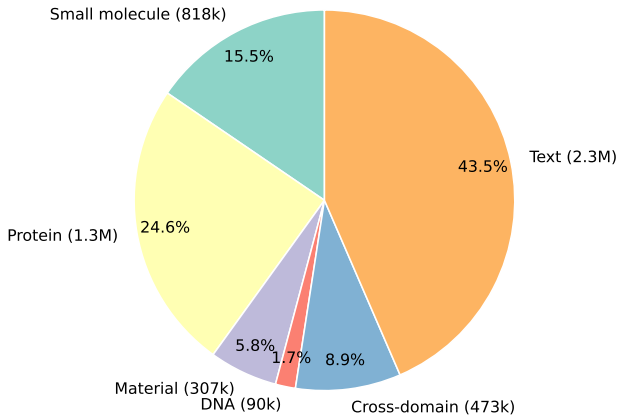


Fig. 5: Statistics of post-training data, measured by the number of sequences.

a consistent training methodology across all three models. The details of the model architecture are provided in Table 2.

Model Parameters	1B	8B	8x7B
Hidden Dimensions	2048	4096	4096
FFN Dimensions	5504	14336	14336
Attention Heads	32	32	32
KV Heads	8	8	32
Number of Layers	16	32	32
Vocabulary Size	130,239	130,239	38,078

Table 2: Model parameters of different sizes of NatureLM.

2.4 Continued pre-training

To address the intricate comprehension required for scientific tasks, NatureLM introduces specific tokens for scientific entities. Consequently, we augment the vocabulary of the chosen LLMs. The embedding weights for these newly introduced tokens are randomly initialized. Directly tuning from pre-training usually causes instability and potentially compromises the language capabilities of the original LLMs. This is primarily due to the introduction of new tokens and the mismatch between the well-trained text tokens and randomly initialized scientific tokens.

To circumvent this issue, we have devised a two-stage pre-training procedure:

Stage 1: Training is exclusively concentrated on the newly introduced tokens. During this phase, the parameters of the existing model are frozen.

This allows the new tokens to adapt to the model gradually, mitigating the risk of instability.

Stage 2: Once the new tokens are adequately trained, we proceed to the second phase where the entire network, including both new and existing parameters, is trained. This joint optimization process ensures that the new tokens are seamlessly integrated with the existing ones, enhancing the model’s overall performance.

This two-stage training approach not only fosters a thorough understanding of the scientific domain but also preserves the integrity and robustness of the underlying language model by preventing potential instabilities. The detailed training recipe is summarized in Table S2.

The validation loss for the three versions of the models is illustrated in Fig. 6. All validation losses decrease as the model size increases. This indicates that larger models are better at capturing the underlying patterns or rules in the data, which is expected due to their increased capacity. The most significant decreases are observed in the text and protein data, suggesting that these datasets benefit more from enlarged models.

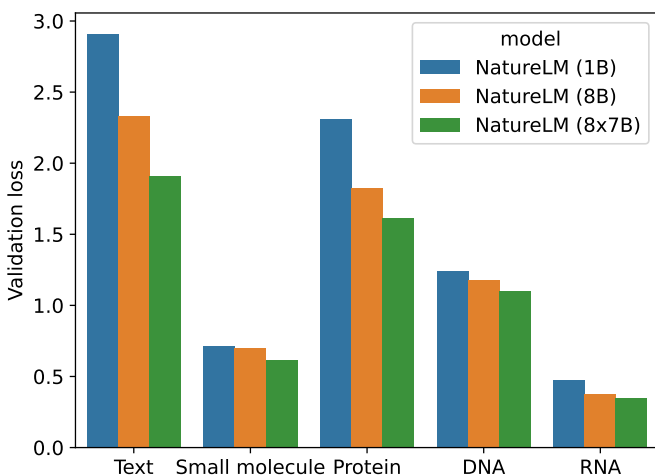


Fig. 6: Validation loss for the 1B, 8B, and 8x7B NatureLM models. Larger models result in smaller validation losses across all domains. NatureLM (8B) is short for “Llama 3 8B NatureLM” throughout this paper.

2.5 Post-training

In the post-training phase, we mainly employ supervised fine-tuning (SFT) using the instruction-response pair data outlined in Section 2.2. These pairs are structured into sequences utilizing the template “Instruction: {instruction}\n\nResponse: {response}” where “{instruction}” and

“`{response}`” serve as placeholders. During the model optimization, the training loss is computed solely on the response part of the sequence. Unlike in the pre-training phase, each sequence contains a single instruction-response pair rather than multiple pairs packed into one sequence. Empirical evidence suggests that this approach aids in stabilizing the post-training process. The 1B and 8B models are trained for 20k steps, while the 8x7B model is trained for 7.8k steps (due to resource constraint). We also explore using RLHF after supervised finetuning and results are discussed in Section 8.1.

2.6 Inference acceleration

As NatureLM will be tested on many downstream tasks, we need to accelerate inference speed to reduce computational cost. We adopted the following approaches: (1) PagedAttention [42], which optimizes LLM serving by partitioning the key-value (KV) cache into fixed-size, non-contiguous blocks, reducing memory fragmentation and enabling efficient memory sharing; and (2) Selective Batching [43], which batches compatible operations while handling attention separately, allowing for flexible and efficient processing of requests with varying input lengths. We employed the vLLM framework [44] to serve NatureLM models, leveraging its implementations of both PagedAttention and Selective Batching. These optimizations were applied to the 1B, 8B, and 8x7B models. Consequently, the inference speed for the NatureLM 8x7B model reached approximately 525 tokens per second with Brain Float 16 (BF16) precision on two NVIDIA A100 GPUs.

3 Small molecule tasks

We assess the capabilities of NatureLM in terms of small molecule generation from the following perspectives:

1. The unconditional generation ability (Section 3.1);
2. The basic properties (such as QED, TSPA, etc.) to small molecule generation (Section 3.2);
3. The translation between small molecule SMILES and IUPAC (Section 3.3);
4. Utilize NatureLM to aid the drug discovery pipeline, which encompasses the generation and optimization of hit compounds (Section 3.4), optimization of binding affinity (Section 3.5), ADMET optimization (Section 3.6), and the synthesis routes of the compounds (Section 3.7).

3.1 Unconditional molecular generation

We input the special token $\langle \text{mol} \rangle$ to NatureLM and let the model generate SMILES. The generation process stops upon encountering the special token $\langle / \text{mol} \rangle$. We assess the validity of the generated SMILES by checking if they can be converted into molecules using RDKit. Additionally, we evaluate the uniqueness of the valid SMILES by calculating the ratio of unique valid SMILES to the total valid SMILES.

The evaluation results are presented in Table 3. The results demonstrate a clear trend: as the model size increases, the performance in terms of validity improves. NatureLM exhibits a consistent increase in uniqueness as the model’s capacity grows. We also establish comparisons between NatureLM and three generalist models: Llama 3 (8B), Mixtral (8x7B), and GPT-4. Our NatureLM significantly outperforms the others in terms of uniqueness. As for validity, the results show that GPT-4 demonstrates a remarkable ability to generalize chemically valid SMILES.

	Validity (%)	Uniqueness (%)
Llama 3 (8B)	77.9	35.1
Mixtral (8x7B)	72.6	35.1
GPT-4	99.6	54.6
NatureLM (1B)	94.9	91.1
NatureLM (8B)	96.8	96.6
NatureLM (8x7B)	98.8	98.8

Table 3: Unconditional evaluation of small molecules generation. RDKit is used to convert the generated SMILES strings into molecular structures and check validity. The uniqueness ratio is calculated among the valid molecules.

3.2 Property-to-molecule generation

The task is to generate molecules with specified properties, which is a critical aspect of molecular design. An example is shown as follows:

Instruction:

Generate a molecule with four hydrogen bond donors.

Response:

```
<mol>C[C@@H](C(=O)O)N)CN=C(N)N</mol>
```

We conduct evaluations of NatureLM on six distinct properties: Quantitative Estimate of Drug-likeness (QED), hydrogen bond acceptors (HBA), hydrogen bond donors (HBD), fraction of sp³ hybridized carbons (FSP3), rotatable bonds (RotBonds), and topological polar surface area (TPSA). All these properties can be calculated using RDKit. For each property, we select multiple values as inputs to the model (see Table S3). We generate 100 molecules for each input and evaluate them with metrics including the Spearman correlation (Fig. 7a) and the correct ratio (Fig. S1). Our findings reveal that on certain property, such as TPSA, the model demonstrates a Spearman correlation greater than 0.8, illustrating the consistency between the generated molecules and the input specifications (Fig. 7b).

Additionally, our model can handle the combination of multiple properties. For example, when given the command “Generate a compound with QED 0.5 and TPSA 40”, the model generates compounds that meet both specified criteria. The results are shown in Fig. 7c. The majority of the generated compounds have QED and TPSA values centered around our desired properties (i.e., 0.5 and 40), demonstrating the versatility and effectiveness of NatureLM in multi-property molecular generation.

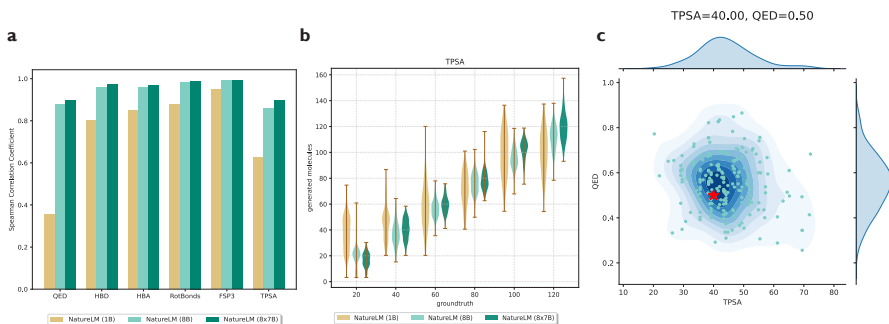


Fig. 7: Evaluation of property-to-molecule generation. (a) Bar plot of the Spearman correlation coefficients between the input property values and generated molecules’ property values. (b) Violin plot showing the input TPSA values and generated molecules’ TPSA values. More properties are shown in Fig. S2. (c) The joint distribution of the generated molecules’ TPSA and QED given the input “TPSA=40, QED=0.5” (see Fig. S3 for more cases).

3.3 Translation between SMILES and IUPAC

We evaluate NatureLM on the translation between SMILES and IUPAC on NC-I2S and NC-S2I [45], the bidirectional IUPAC-SMILES translation dataset comprising 2993 pairs of SMILES and their corresponding IUPAC names (Table 4). We ensure that there is no test set leakage in this setting. On both text-to-SMILES and SMILES-to-text translation tasks, NatureLM (8x7B) outperforms all competing language models in terms of accuracy, demonstrating our model’s strong capability for text-molecule correspondence. NatureLM significantly outperforms GPT-4 and Claude 3 Opus [46], strong generalist large language models (LLMs), highlighting the necessity of training on scientific data. Compared with another LLM trained on text and SMILES corpus LlaSMol_{Mistral} [45], NatureLM also obtains significantly better performance. Moreover, NatureLM (8x7B) performs comparably with STOUT [47], the widely-used model trained specially for IUPAC-SMILES translation task, demonstrating NatureLM’s potential as a scientific generalist in specific domains. The performance increases from NatureLM (1B) to NatureLM (8x7B), exhibiting the scaling benefits of larger models. A case study is presented in Fig. S9, comparing NatureLM with general large language models and highlighting the advantages of NatureLM in scientific tasks.

	IUPAC-to-SMILES	SMILES-to-IUPAC
STOUT	0.735	0.565
GPT-4	0.033	0
Claude 3 Opus	0.177	0
LlaSMol _{Mistral}	0.701	0.290
NatureLM (1B)	0.476	0.284
NatureLM (8B)	0.679	0.517
NatureLM (8x7B)	0.704	0.607

Table 4: IUPAC-SMILES translation results. Models are evaluated by top-5 accuracy.

3.4 Target-aware hit compound generation and optimization

The task is to generate small molecule compounds given the target protein sequence. The combination of NatureLM and structure-based compound design, such as TamGen [48] and TargetDiff [49], will be explored in the future. We test NatureLM within two distinct scenarios:

(1) Generate compounds from the target protein sequences. This process is crucial for the hit identification stage of drug discovery, with the goal of discovering chemical entities that exhibit specific interactions with the target protein.

(2) Generate molecular fragments based on the target protein sequences and partial molecular structures as inputs. This method is instrumental during the lead optimization phase, where we scrutinize and refine the molecular architecture to improve efficacy and precision.

The examples are shown below:

▷ *Scenario 1*: Complete molecule generation

Instruction:

Produce a compound guided by the target

`<protein>LALSLTADQMVSALL...SYDLLLEMLDAH</protein>`

Response:`<mol>CC1=C(c2cccc(O)c2)C(c2ccc(I)cc2)Oc2ccc(O)cc21</mol>`

▷ *Scenario 2*: Fragment generation

Instruction:

Design a compound with reference to the target

`<protein>DTKEQRILR...EKAIYQGP</protein>` and the fragment

`<fragA>O=c1[nH]cnc2c(O)cc([*:1])c([*:2])c12</fragA>`

Response:

`<fragB>Fc1ccc([*:1])cc1.Fc1ccc([*:2])cc1</fragB>`

Here, “[*:digit]” refers to the connection point of the molecular fragment, like the R1 and R2 in Fig. 8.

In the first scenario, we compare NatureLM with a sequence generation method, TamGen [48], and two other approaches that design compounds in 3D space based on the input target structure: a diffusion-based method, TargetDiff [49], and an autoregressive generation method in 3D space, Pocket2Mol [50]. We follow the evaluation procedure outlined in the TamGen paper [48], which includes calculating the docking score using AutoDock Vina [51, 52], as well as assessing the QED, synthetic accessibility scores (SAS), diversity of the generated compounds, the percentage of compounds with logP in the range [0,5], and the percentage of compounds satisfying the rule-of-five. The results are presented in Table 5. We can see that in terms of docking score, QED and synthesis ability, NatureLM surpasses previous baselines, highlighting its effectiveness. For the other metrics, NatureLM achieves comparable performance to the baselines.

	Vina (↓)	QED	SAS	Diversity	LogP ∈ [0, 5]	Ro5
Pocket2Mol	-4.90	0.52	0.84	0.87	0.76	1
TargetDiff	-6.08	0.55	0.67	0.83	0.74	0.98
TamGen	-6.66	0.56	0.76	0.75	0.84	0.99
NatureLM (1B)	-6.80	0.64	0.82	0.77	0.85	0.99
NatureLM (8B)	-6.92	0.62	0.81	0.73	0.84	0.99
NatureLM (8x7B)	-6.95	0.62	0.82	0.75	0.84	0.99

Table 5: Statistics of target to complete compound sequence generation.

Additionally, we utilize NatureLM for fragment generation. We selected three papers published after May 2024 [53–55], where part of their task is to solve the issue of compound optimization. From these papers, we choose the target proteins and the fragments to retain, allowing NatureLM to generate the remaining fragments. The results are illustrated in Fig. 8. In this instance, it is evident that larger NatureLM models yield superior docking scores in general.

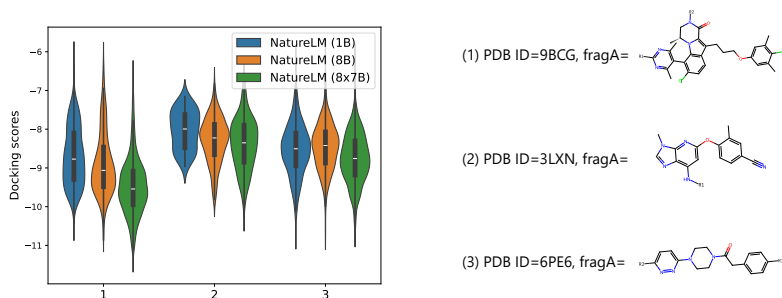


Fig. 8: Docking scores for molecules in target-to-fragment generation. This violin plot presents the docking scores of molecules involved in target-to-fragment generation. We selected three recent papers that focus on fragment optimization: [54], [55] and [53], which utilize PDB IDs 9BCG, 3LXN, and 6PE6, respectively. The input fragment is visualized alongside its corresponding PDB ID for clarity.

3.5 Text-guided binding affinity optimization

To further improve the binding affinity between a target and a molecule, we propose a text-guided binding affinity optimization task. Given a target name and a molecule with a known binding affinity for that target, we aim to generate molecules with higher binding affinity, which is a crucial component for lead optimization. An example is shown below:

Instruction:

Improve the binding affinity on Uridine-cytidine kinase 2 of
<mol>Cc1ccc(-c2nc3c(c(SCC(=O)Nc4cccc4)n2)Cc2cccc(C)c2O3)cc1</mol>

Response:

<mol>Cc1ccc(-c2nc3c(c(SCC(=O)Nc4cccc(C(=O)O)c4)n2)Cc2cccc(C)c2O3)cc1</mol>

Here, the target information is provided in text format, which complements the FASTA representation used in Section 3.4. We will combine text and FASTA in the future.

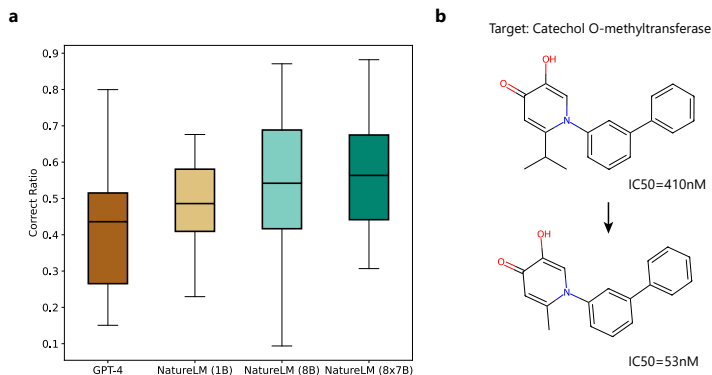


Fig. 9: Evaluation of text-guided binding affinity optimization. (a) Box plot of the correct ratios of GPT-4, NatureLM (1B), NatureLM (8B) and NatureLM (8x7B) on 12 targets. (b) A case on the binding affinity optimization for Catechol O-methyltransferase. With small modifications, the binding affinity improves from 410nM to 53nM.

We test NatureLM on 12 targets that are not present in the post-training data and use a hybrid retrieval and docking approach for evaluation. Specifically, for the generated molecules, if we can retrieve their binding affinity values from the ChEMBL database, we compare these values with the original molecule’s binding affinity. Otherwise, we resort to docking scores as the comparison metric. For the 12 selected targets, their Spearman correlation between the docking score and the actual binding affinity for known molecules exceeds 0.5, indicating the reliability of using docking for assessment (Table S4).

We observe that NatureLM can successfully improve the molecule’s binding affinity by making modifications on its chemical components, in a manner similar to what a chemist would typically do (Fig. 9b). Compared with GPT-4, NatureLM can generate molecules (Fig. 9a) with higher binding affinity, making it a better tool for molecule optimization than general purpose LLM. Another observation is that more than 90% molecules generated by NatureLM do not have known binding affinity score in ChEMBL database. For 8 out of the 12 targets, over 50% of the generated novel molecules successfully improved the docking scores (Fig. S4), demonstrating the model’s potential in exploring chemical spaces and discovering novel drugs. We observe that NatureLM (8x7B) and NatureLM (8B) outperform NatureLM (1B) as they generate more correct molecules for the majority of targets (Fig. S5).

3.6 Text-guided metabolism & distributional property optimization

We next assess the molecular optimization capabilities of NatureLM regarding metabolism and its potential to cross the blood-brain barrier (BBB), a crucial factor in drug distribution. For metabolism, the goal is to reduce the inhibition of five key metabolic enzymes: CYP1A2, CYP2C19, CYP2C9, CYP2D6 and CYP3A4. An example is shown below:

Instruction:

Transform <mol>COCCn1c(=O)c(-c2ccccc2)nc2cnc(N3CCOCC3)nc21</mol> to yield lower CYP1A2 inhibition and present a better metabolic safety record.

Response:

<mol>COc1ccc(-c2nc3cnc(N4CCOCC4)nc3n(Cc3cccc(OC)c3)c2=O)cc1</mol>

In terms of BBB permeability (BBBP), we evaluate the enhancement BBB permeability. An example is provided below:

Instruction:

Adjust the molecule <mol>CC[C@H](NC(=O)c1c(OCCCC(=O)O)c(-c2ccccc2)nc2ccccc12)c1ccccc1</mol> to facilitate its passage through the blood-brain barrier.

Response:

<mol>CC[C@H](NC(=O)c1c(O)c(-c2ccccc2)nc2ccccc12)c1ccccc1</mol>

For each test sample, we used random search to generate four cases. To determine whether NatureLM effectively refined the input molecule, we trained six groups of deep learning models for this evaluation. For assessing BBBP, we utilized the state-of-the-art model, BioT5 [56], to determine whether a compound is capable of crossing the BBB. For metabolism optimization, we used ChemProp [57] to train classifiers to test if a molecule has the ability to inhibit enzymes from the cytochrome P450 (CYP) superfamily. We evaluated the percentage of molecules that were successfully optimized according to the specified criteria (see Section C.4 for details).

Table 6 displays the outcomes of BBBP and metabolism optimization. The success rates for optimizing BBBP with the 1B, 8B, and 8x7B versions of NatureLM are 0.482, 0.549, and 0.552, respectively. Larger models show better performance, suggesting potential for enhancement opportunities in the future. For metabolism optimization, generally, the 8B model outperforms the others in terms of success rate, followed by the 8x7B model and lastly the 1B model. The 1B and 8B models share the same architecture (dense models, large vocabulary size), whereas the 8x7B model has a distinct one (mixture-of-expert model, relative small vocabulary size). In this particular task, the progression from the 1B model to the 8B model is consistent. However, a detailed analysis contrasting the 8x7B model is to be conducted in subsequent studies. Additionally, we jointly optimized metabolism and a basic property.

The findings indicate that larger models generally yield better results (see Table S5).

	BBBP	CYP1A2	CYP2C19	CYP2C9	CYP2D6	CYP3A4	CYP Average
1B	0.482	0.805	0.815	0.770	0.750	0.831	0.794
8B	0.549	0.882	0.813	0.882	0.833	0.913	0.865
8x7B	0.552	0.837	0.834	0.838	0.812	0.853	0.835

Table 6: Optimization results of BBBP metabolism and CYP enzymes. Measured by success rate.

3.7 Retrosynthesis prediction

Retrosynthesis aims to identify synthesis routes for target molecules using commercially available compounds as starting points, a critical task in the discovery and manufacture of functional small molecules [58–60]. The applicability of ML-based retrosynthesis tools largely depends on the accuracy of single-step retrosynthesis prediction. We evaluate the capability of NatureLM for single-step retrosynthesis prediction on USPTO-50K [61]. NatureLM is prompted with the task description and the chemical SMILES of the product molecule, and is expected to generate potential reactants.

We followed the common practice for splitting the USPTO-50K dataset [62, 63], and evaluated the performance using the 5007 reactions included in the test set. We ensured that there is no test set leakage in this setting. As outlined in Table 7, all sizes of NatureLM models surpass other methods in terms of top- k accuracy, demonstrating our model’s accurate predictive ability for retrosynthesis prediction. NatureLM significantly outperforms GPT-4, suggesting that training on scientific data is crucial for models to excel in scientific tasks. Furthermore, NatureLM outperforms the state-of-the-art domain-specific models such as LocalRetro [64] and R-SMILES [65], showing NatureLM’s potential as a scientific generalist in critical scientific tasks. We also note an increase in performance from NatureLM (1B) to NatureLM (8x7B), demonstrating the scaling advantages of larger models.

Instruction:

Please suggest possible reactants for the given product
`<product>CC(=O)c1ccc2c(ccn2C(=O)OC(C)(C)C)c1</product>`

Response:

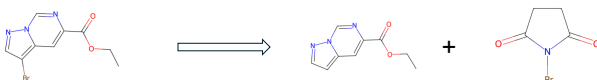
`<reactant> CC(=O)c1ccc2[nH]ccc2c1.CC(C)(C)OC(=O)OC(=O)OC(C)(C)C</reactant>`

We selected a newly discovered reaction from a U.S. patent with ID US12018024B2 (granted to Novartis on June 25, 2024) as the case study. As shown in Figure 10, the product is a brominated heterocyclic compound. To synthesize such molecules, organic chemists typically begin by constructing the

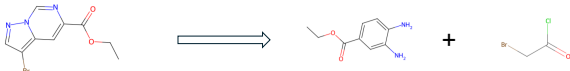
	Top-1 accuracy	Top-3 accuracy
GPT-4	22.4%	N/A
LocalRetro [64]	51.5%	76.5%
R-SMILES [65]	56.0%	79.1%
EditRetro [66]	60.8%	80.6%
NatureLM (1B)	68.6%	86.8%
NatureLM (8B)	70.2%	85.9%
NatureLM (8x7B)	71.9%	87.4%

Table 7: Retrosynthesis prediction results on USPTO-50K dataset.

1) By NatureLM/Reference



2) By DeepSeek-R1



3) By o3-mini-high

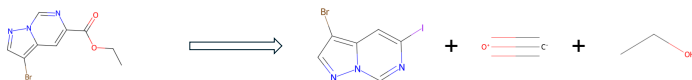


Fig. 10: Case study on retrosynthesis prediction. We evaluated the performance of NatureLM, DeepSeek-R1, and o3-mini-high for retrosynthesis prediction using a reaction from U.S. Patent ID US12018024B2 (not included in our training set), granted to Novartis on June 25, 2024. NatureLM successfully proposed the ground-truth reactants from the patent, while the outputs from the other two methods required further refinement to achieve the same level of accuracy.

ring system, then followed by a halogenation reaction on the ring. The halogenated site is subsequently used in further syntheses, often coupling with other ring systems. In this context, our NatureLM model accurately predicted one of the most common brominating agent NBS (*N*-Bromosuccinimide) in this step, aligning perfectly with experimental results. DFT optimization calculations to reactant CCOC(=O)c1cc2ccnn2cn1 show that 3-position is the most nucleophilic. So bromination prefers at 3-position. This demonstrates NatureLM’s capability to effectively predict useful reactants in chemical reactions.

In contrast, DeepSeek-R1 [12] model selected incorrect reactants. DeepSeek-R1 focused on constructing a heterocyclic ring system in this step. However, it incorrectly positioned the nitrogen and carbon atoms in the substrate, leading to the wrong outcome. Meanwhile, o3-mini-high model selected another correct route but not so convenient for the whole synthetic

process. o3-mini-high might attempt to construct the acetyl side chain by transition-metal-catalyzed CO insertion reaction. Although radical mechanism can achieve this since iodo atom is more reactive than bromo atom, introducing the side chain at this stage may still lead to a side reaction at the bromo atom. In the actual synthesis, this acetyl side chain is generally constructed in previous steps. These cases illustrate that, so far, general LLMs cannot fully grasp the rationale behind chemical synthesis. Although they can generate some reasons and predictions, these do not align with practical strategies.

Another example is shown in Fig. S10, where NatureLM accurately predicts the reactants, while the outputs from DeepSeek-R1 and o3-mini-high require additional refinement.

4 Protein tasks

Our model’s capabilities with respect to proteins are assessed through several distinct types of tasks:

1. Unconditioned protein generation: The model generates protein sequences from scratch without any specific conditions or prompts.
2. Text-guided protein generation: This task involves guiding the model to generate protein sequences based on given natural language descriptions.
3. Antibody design: The model designs the Complementary-Determining Region H3 (CDR-H3) of antibodies to effectively bind to target antigens.
4. Protein characteristics description generation: This task is to generate clear, human-readable explanations of protein sequences, describing their properties and functions.
5. Case study: The model designs heme-binding protein design driven by text and SMILES.

4.1 Unconditioned generation

The first capability of the model is generating protein sequences from scratch freely, prompted by the start token for proteins only, i.e., $\langle \text{protein} \rangle$. However, since there is no golden standard for evaluating proteins when no conditions are specified, it is difficult to assess the generation results. We focus on foldability, measured by pLDDT score [67], as well as lengths and diversity of the sequences, for the valid sequences.

Model	Avg Length	Diversity	AVG pLDDT
Mixtral 8x7b	53	0.906	69.9
GPT-4	46	0.816	65.1
NatureLM (1B)	288	0.985	69.8
NatureLM (8B)	285	0.973	71.8
NatureLM (8x7B)	318	0.989	75.9

Table 8: Protein Sequence Generation Comparison. The average length of natural proteins (calculated from a subset of proteins randomly sampled from UR50) is about 311. The diversity was calculated by the number of clusters with 50% sequence identity divided by the total generated sequence count. The pLDDT scores were calculated by OmegaFold [68] on the generated sequences with length less than 100 for a fair comparison. The length distribution is shown in Figure S14.

As shown in Table 8, NatureLM consistently outperform Mixtral 8x7b and GPT-4 in terms of average sequence length, diversity, and average pLDDT score. The NatureLM (8x7B) model achieves the best performance across all metrics, with an average length of 318, diversity of 0.989, and average pLDDT

score of 75.9. ProLLAMA [24], a fine-tuned LLM for protein, generates proteins without explicitly defined constraints on length, achieving a pLDDT score of 66.5. In contrast, our approach, which does not impose length constraints, results in pLDDT scores of 69.8 and 78.1 for the 8B and 8x7B models, respectively, demonstrating our significant advancement in protein sequence generation.

4.2 Text-guided protein generation

For text-guided protein generation, we evaluated our models’ ability to generate proteins with specific properties based on natural language prompts. In this study, we focused on two key properties: solubility and stability, leaving the exploration of additional properties for future work. For stability, the models were tasked with generating protein sequences that exhibit stable properties. Regarding solubility, since both soluble and insoluble proteins exist in nature, we instructed NatureLM to generate sequences of both types. Sample prompts are shown below, and a full list of prompts can be found in Figure S16.

- ▷ An example prompt for “stable protein generation”
I require a stable protein sequence, kindly generate one.
- ▷ An example prompt for “soluble protein generation”
Generate a soluble protein sequence.
- ▷ An example prompt for “insoluble protein generation”
Produce a protein sequence that is not soluble.

To evaluate the stability and solubility of a generated protein sequence, we utilized two specialist models fine-tuned from the protein foundation model, SFM-Protein [69], as oracle models. One model was used for stability classification, while the other was used for solubility classification. The oracle models provide probabilities that suggest the likelihood of the sequence possessing the desired property. To verify the efficiency of our model against random sampling, we have also chosen a subset of 1000 natural protein sequences from the UR50 dataset and assessed them using the same oracle models.

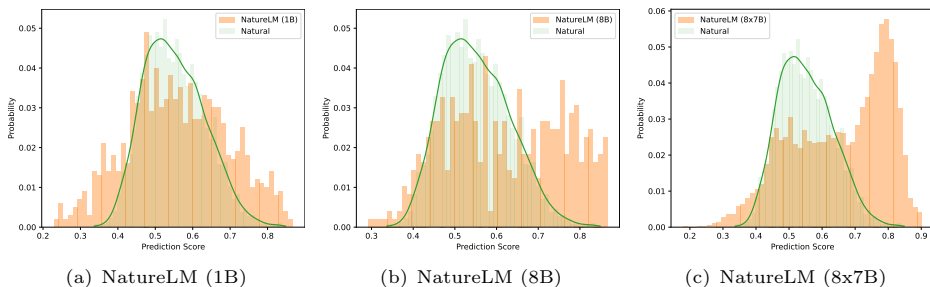


Fig. 11: Stability score distribution of the generated sequences.

Source	AVG Prediction	Data Ratio (Score > 0.5)
Natural	0.552	0.704
NatureLM (1B)	0.559	0.644
NatureLM (8B)	0.619	0.757
NatureLM (8x7B)	0.655	0.812

Table 9: Stability score ratio of the generated sequences.

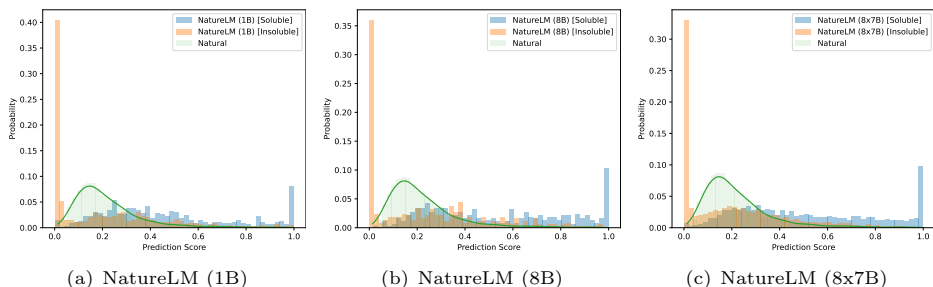


Fig. 12: Solubility score distribution of the generated sequences.

Figures 11 and 12 show the distributions of stability and solubility scores for the generated sequences, respectively. The NatureLM models demonstrate controlled distribution shift in generating proteins with desired properties compared to the natural sequences. In the task of generating more stable proteins, as shown in Figure 11, a clear trend emerges: as the model size increases, the proportion of sequences classified as stable grows, with a pronounced peak in the NatureLM (8x7B) results. The quantified data, summarized in Table 9, further supports this observation. All three models produce proteins that are more stable than natural sequences based on average stability scores. Additionally, two of the models outperform natural proteins in terms of the number of sequences that exceed a stability threshold of 0.5. For the solubility condition, Figure 12 reveals a similar trend. As the model size increases, the separation between the distributions of soluble and insoluble scores becomes more distinct, with less overlap.

4.3 Antigen-binding CDR-H3 design

The task of antigen-binding CDR-H3 design focuses on constructing the Complementary-Determining Region H3 (CDR-H3) of an antibody to bind effectively to a target antigen. We employed the RAbD benchmark dataset [70], comprising 60 antibody-antigen complexes. The example is shown below:

Instruction:

Using antigen `<protein>TQVCTGTDMKLR...GESSEDCQS</protein>`
and antibody frameworks `<antibody>IVLTQTPS...LAVYYC</antibody>`

and `<antibody>FGGGTRLEIEVQ</antibody>`, create the CDR3 regions.

Response:

`<antibody>QQYSNYPWT</antibody>`

The generation quality is evaluated by the Amino Acid Recovery (AAR) scores for the CDR-H3 design task. We use r and \hat{r} to represent the reference and generated sequences respectively, while $L(r)$ and $L(\hat{r})$ denote the number of amino acids in r and \hat{r} . The i -th residue in the two sequences is denoted by r_i and \hat{r}_i . The AAR is defined as follows:

$$\text{AAR}(r, \hat{r}) = \frac{1}{L(r)} \sum_{i=1}^{L(r)} \mathbb{I}(r_i = \hat{r}_i). \quad (1)$$

In case $L(\hat{r}) > L(r)$, only the first $L(r)$ elements are verified. If $L(\hat{r}) < L(r)$, we assign $\mathbb{I}(r_i = \hat{r}_i) = 0$ for $i > L(\hat{r})$.

Method	AAR (\uparrow)
GPT-4	0.312
RefineGNN [71]	0.298
HSRN [72]	0.327
MEAN [73]	0.368
ABGNN [74]	0.396
Llama 3 (8B)	0.275
NatureLM (1B)	0.273
NatureLM (8B)	0.368
NatureLM (8x7B)	0.376

Table 10: AAR of the CDR-H3 design. Please note that the NatureLM models utilize sequence-only input for this task, whereas the baseline models may incorporate additional information, such as structural data.

Table 10 presents the Amino Acid Recovery (AAR) scores for the CDR-H3 design task. As the model size of NatureLM increases, the AAR gradually increases. The NatureLM (8x7B) model achieves competitive performance with an AAR of 0.376, outperforming several specialized GNN-based models, except ABGNN [74] in our study. While SFM-protein, a BERT-like model trained on protein sequences, holds the top performance, our results demonstrate the potential of NatureLM in CDR-H3 design, particularly as the model scales and undergoes further refinement.

4.4 Protein characteristics description generation

Despite the rapid discovery of natural protein sequences facilitated by advanced sequencing techniques, the functions of many of these proteins remain largely unknown. This knowledge gap restricts our ability to exploit

these proteins for engineering and therapeutic purposes. In this study, we explored the annotation generation capabilities of the NatureLM series.

To achieve this, we compiled pairs of protein sequences and their human-readable annotations from various species, sourced from the NCBI database. We divided the dataset temporally. Model performance was evaluated using Rouge-L scores. As shown in Table 11, NatureLM models consistently outperformed Llama 3 8B in Rouge-L scores, with performance differences widening as model size increased. Notably, the NatureLM (8x7B) model achieved the highest score of 0.585. A detailed analysis presented in Figure 13 revealed that the NatureLM (8x7B) model not only generates protein annotations with higher accuracy but also successfully identifies orthologues and functions of proteins, while NatureLM (8B) is also able to generate reasonable results in many cases.

Model Setting	Rouge-L
GPT-4o	0.091
Fine-tuned Llama 3 (8B)	0.324
NatureLM (1B)	0.548
NatureLM (8B)	0.572
NatureLM (8x7B)	0.585

Table 11: Performance of protein description generation, measured by Rouge-L. Llama 3 (8B) serves as a baseline, which is directly fine-tuned on the data collection described in Section 2.2. More details about this baseline in Section 10.

In conclusion, NatureLM demonstrates strong performance across a wide range of protein-related tasks, from unconditioned generation to specific design tasks like CDR-H3 design. The scalability of our approach is evident, with larger models consistently outperforming smaller versions and often achieving state-of-the-art results.

4.5 Heme-binding protein design driven by text and SMILES

NatureLM is capable of designing proteins to meet various requirements. In this case study, we demonstrate how to use NatureLM to design a protein that binds to heme cofactor.

Heme is an essential molecule, playing critical roles in oxygen transport and various enzymatic processes. Designing a protein that can bind to heme can contribute to advancements in therapeutic development, biochemical research, and synthetic biology.

The protein design practice is outlined as the following 4 steps:

Step 1: protein generation. We prompt NatureLM to generate proteins using two approaches:

Gene ID	834896	68201	161973
Reference	Member of putative ligand-gated ion channel subunit family	Orthologous to human ccdc34 (coiled-coil domain containing 34).	Orthologous to human fbxo15 (F-box protein 15).
Llama 3 (8B)	contain amino acid sequence motifs characteristic of ATP-binding cassette (ABC) transporters.	Orthologous to human FAM107A (family with sequence similarity 107 member A).	Is expressed in germline cell.
NatureLM (1B)	Orthologous to human SLC25A37 (solute carrier family 25 member 37).	Orthologous to human CCDC74A (coiled-coil domain containing 74A) and CCDC74B (coiled-coil domain containing 74B).	Orthologous to human C2orf71 (chromosome 2 open reading frame 76).
NatureLM (8B)	Encodes a plasma membrane protein involved in the positive regulation of organ size development. Overexpression results in organ size enlargement.	Orthologous to human CCDC34 (coiled-coil domain containing 34).	Orthologous to human FBXW12 (F-box and WD repeat domain containing 12).
NatureLM (8x7B)	member of Putative ligand-gated ion channel subunit family	Orthologous to human CCDC34 (coiled-coil domain containing 34).	Orthologous to human FBXO15 (F-box protein 15).

Fig. 13: Generated descriptions for different proteins.

1. Text-based protein design, where we provide a text instruction (here in English);
2. Small-molecule-based protein design, where we use the SMILES representation of heme as part of the input instruction.

Examples of these prompts and their corresponding responses are shown below:

▷ Generate proteins based on text (Section 4.2)
Instruction: Design a heme-binding protein sequence.
Response: <protein>MSAAEGAVVFSEEKEALVLK...</protein>
▷ Generate proteins based on the SMILES of the heme
Instruction: Generate a protein that can bind to
<mol>[Fe+2].C=CC1=C(C)c2cc3[n-]c(cc4[n-]c(cc5nc(cc1n2)C(C)...</mol>
Response: <protein>ETIGKRVFVHYCHGCHSQNALGI...</protein>

Step 2: description generation. For each generated protein, we utilize the protein-to-text functionality in NatureLM (Section 4.4), to obtain a description of the properties and potential functions of the generated protein.

Step 3: screen proteins through keyword matching. In this step, we use GPT-4o to generate a keyword list, called **HemeList**, containing characteristics associated with heme-binding proteins. For every protein description generated in Step 2, we check whether it contains keywords from **HemeList**. If a description matches these criteria, the corresponding protein is added to a list called **HemeProtein**.

Step 4: structure prediction and validation. For each protein in **HemeProtein**, we use Protenix [75] to predict the complex structure of the generated proteins bound to heme. The predicted structures are then inspected to

ensure that the proteins can form the critical interaction with heme for stable binding.

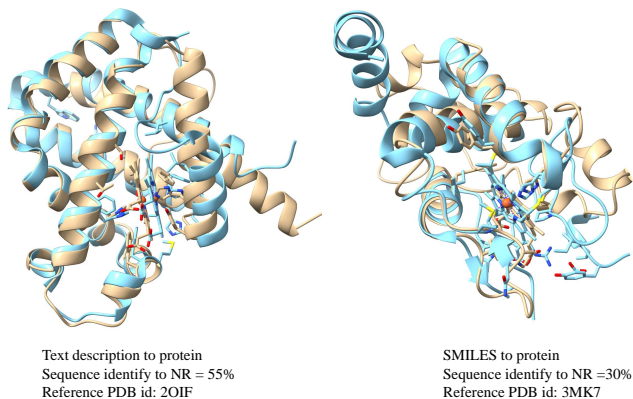


Fig. 14: Two examples of proteins with plausibility of binding to heme. The yellow models represent the generated protein structures, while the blue models correspond to the reference structures retrieved using the built-in “blast protein” function in ChimeraX [76]. In each model, the heme binding region is highlighted by showing the nearby residues in stick representations. We use the protein-to-text functionality of NatureLM to generate functional annotations for these proteins, and the original outputs are provided here: (left protein) “Heme-binding protein”; (right protein) “Transfers electrons from cytochrome c551 to cytochrome oxidase; C-type cytochrome; Part of the cbb3-type cytochrome c oxidase complex.”

In the text-based design case study (Fig.14 left), two histidine residues are positioned in close proximity to the iron located in the center of heme, enabling the formation of coordinated bonding interactions with the heme group. Similarly, in the SMILES-based design, the NatureLM generates proteins with binding motifs similar to those generated in the text-based example (Fig. S11). However, as shown in Fig. 14 (right), we show a representative case where a methionine and histidine residue are observed to interact closely with the iron ion (see Fig. S12 for more discussion on this case). These residues effectively coordinate the metal ion through their respective side chains, demonstrating alternative structural strategies for heme binding. Furthermore, the designed protein sequences differ significantly from those present in the database, indicating that NatureLM can generate novel sequences with distinct structural properties. Collectively, these results demonstrate the effectiveness of NatureLM in designing functional heme-binding proteins with diverse and novel structural features. We also compare the apo and holo structures of the generated proteins in Fig. S13, which shows that the key residues involved in

34 CONTENTS

heme binding, such as histidine and methionine, occupy similar positions in both structures.

5 Material tasks

To evaluate the capabilities of NatureLM for material generation, it is prompted to generate material’s compositions in both unconditional and conditional way. For unconditional generation, the model is prompted with a special token indicating the start of material (i.e., $\langle \text{material} \rangle$) and is expected to generate the composition of the material (Section 5.1). For conditional generation, the model is prompted to generate material formula and structure under specific human instructions, including: (1) Material generation for given composition (Section 5.2); (2) Material generation for desired properties (Section 5.3).

Crystal structures are fundamental to determining the physical, chemical, and mechanical properties of materials. Complementing the sequence outputs of NatureLM, we finetune NatureLM into a specialized model, NatureLM-Mat3D, which predicts crystal structures from the generated chemical formulas (see Section 5.4). After generating material formulas and space groups with NatureLM, we then utilize NatureLM-Mat3D to convert them into crystal structures for further evaluation and practical application.

5.1 Unconditional material generation

The model is tasked with generating materials with arbitrary compositions. The input to NatureLM is $\langle \text{material} \rangle$, and it produces material compositions with a specified space group. An example is provided below,

Instruction: $\langle \text{material} \rangle$
Response: $\langle \text{material} \rangle$ A A B B B $\langle \text{sg12} \rangle \langle / \text{material} \rangle$

where A, B refer to elements and $\langle \text{sg12} \rangle$ denotes the space group.

We evaluated the SMACT validity of the generated materials. Furthermore, we utilized NatureLM-Mat3D to predict the crystal structures of a randomly selected subset of valid compositions. The energy above hull (abbreviated as ehull) of the predicted structures was then evaluated using MatterSim [77]. The distribution of ehull is shown in Fig. S6. We also assessed the ratio of stable materials, defining a generated material as stable if its ehull < 0.1eV/atom. The results are presented in Table 12. It is evident that as the model size increases, the SMACT validity and stability of the generated materials improve.

Model	SMACT (%)	Stability (%)
NatureLM (1B)	49.20	10.12
NatureLM (8B)	63.42	12.47
NatureLM (8x7B)	66.07	17.86

Table 12: The SMACT validity and stability (with ehull < 0.1eV/atom) for unconditional material generation. The distribution of ehull for the generated materials is illustrated in Fig. S6.

5.2 Material generation for given composition

The model is tasked with generating materials containing specific elements:

Instruction: Build a material that has Li, Ti, Mn, Fe, O
Response: `<material>` Li Li Li Li Ti Ti Ti Mn Mn Fe Fe Fe O O O O
 O O O O O O O O O O O `</material>`

We evaluated the SMACT validity, stability, novelty, and precision of the generated materials. The novelty is measured as the ratio of unique generated materials that are not present in our instruction tuning data. The composition precision is calculated as

$$\text{composition precision} = \frac{1}{N} \sum_{i=1}^N \frac{|E_{pi} \cap E_{gi}|}{|E_{pi}|}, \quad (2)$$

where E_{pi} and E_{gi} stand for the sets of elements in the i -th prompt and corresponding generated material respectively.

The results are demonstrated in Table 13, and the distribution of ehull is depicted in Figure 15. Table 13 shows a significant improvement in SMACT validity scores due to instruction tuning compared to unconditional generation. The precision for all three models is close to 100%, indicating their strong capability to follow language instructions for generating material formulas with expected elements. Additionally, the high novelty demonstrates the models' generative abilities. Furthermore, stability improves with model size, highlighting their scalability. Figure 15 illustrates this more clearly: as model size increases, the ehull distribution shifts closer to zero, indicating that more materials have lower energy and are in a more stable state.

Model	SMACT (%)	Stability (%)	Precision (%)	Novelty (%)
NatureLM (1B)	79.38	31.56	97.95	97.13
NatureLM (8B)	83.36	35.56	98.44	95.51
NatureLM (8x7B)	81.56	36.46	97.68	94.83

Table 13: The SMACT validity, stability, precision, and novelty for composition to material generation.

5.3 Material generation for desired properties

NatureLM can generate materials with desired properties, and here we demonstrate this capability by generating materials that have specific bulk modulus. The bulk modulus of a substance is a measure of the resistance of a substance to bulk compression. As a proof-of-concept, the NatureLM is prompted to generate materials with the following instructions:

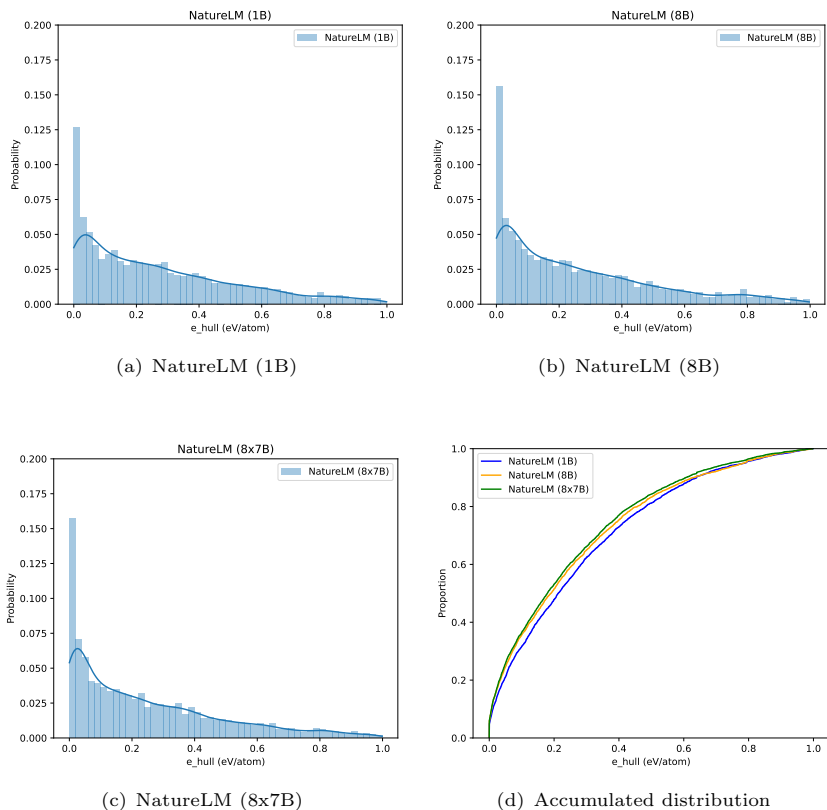


Fig. 15: Energy above hull (ehull) distribution for composition to material generation.

Instruction: Construct the composition for a material with a specified bulk modulus of 86.39 GPa.

Response: `<material> Se Se Pd Sc <sg164></material>`

We evaluated the SMACT validity, stability, novelty, and precision of the generated materials. Success rate is defined as the ratio of generated materials whose bulk modulus is within 10% of the instructed value, compared to other generated materials.

The results in Table 14 indicate improved SMACT validity and stability as the model scales. Figure S7 depicts the distribution of ehull for the generated materials, showing a shift closer to zero with increasing model size.

Further, to demonstrate how NatureLM follows the instruction to generate materials with expected bulk modulus, we depict the distribution of the bulk modulus of generated materials under the instructions in Figure 16 where the x -axis denotes the bulk modulus in the instruction prompt and the y -axis denotes the predicted bulk modulus of the generated materials calculated by

MatterSim. We can see that, as the model scales, the distribution aligns more closely with the ideal linear diagonal.

To assess how many novel materials NatureLM can generate, we prompted the model with a single instruction and allowed it to produce up to 1,000,000 material formulas. We then plotted the count of novel material formulas against the total number generated. Novel materials are defined as those passing the SMACT validity check, not present in the instruction tuning data, and not previously generated. Figure S8 shows that the number of novel materials increases with the total generated. Even at 1 million generated materials, novel ones continue to appear, highlighting the model’s strong generative capability.

Model	SMACT (%)	Stability (%)	Precision (%)	Novelty (%)
NatureLM (1B)	86.76	39.34	40.00	52.38
NatureLM (8B)	87.21	52.81	44.06	36.31
NatureLM (8x7B)	94.75	53.60	44.62	32.42

Table 14: The SMACT validity, stability, precision, and novelty of generated materials conditioned on bulk modulus.

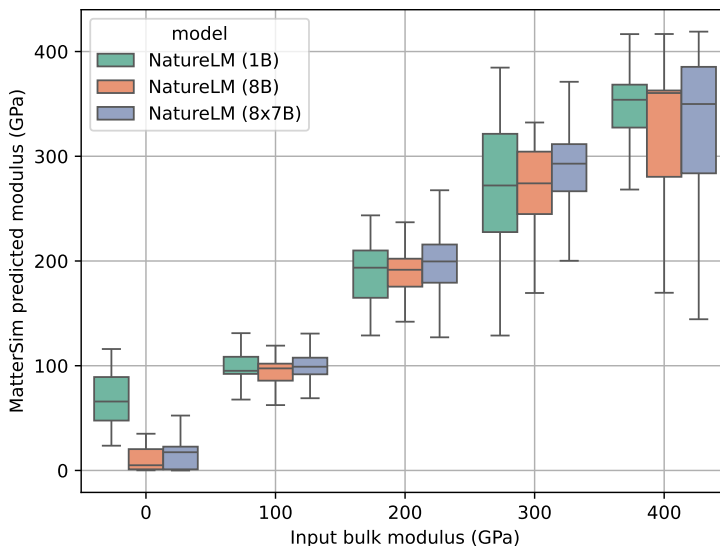


Fig. 16: Distribution of predicted bulk modulus values for generated materials. The x -axis represents the input bulk modulus values from the instructions, while the y -axis shows the predicted values for the generated molecules calculated by MatterSim.

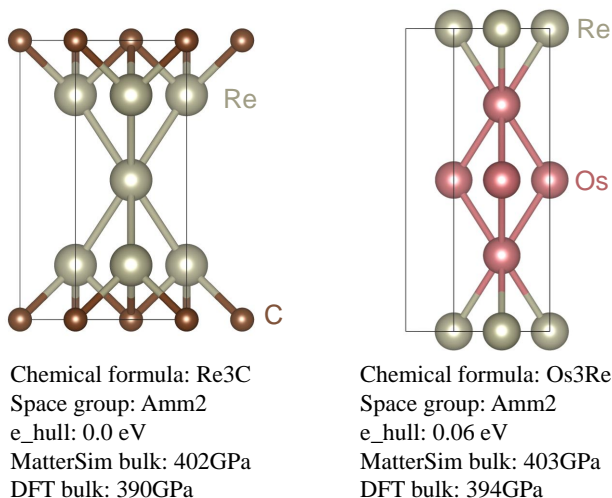


Fig. 17: Two cases with bulk modulus values near 400 GPa (evaluated via DFT) were identified. The chemical formulas, space groups, energy above the hull (e_{hull}), and bulk modulus values obtained from MatterSim and DFT calculations are provided.

Materials with an ultra-high bulk modulus are highly sought after due to their exceptional stiffness and incompressibility, making them indispensable for applications in extreme environments, such as aerospace, industrial tooling, and advanced engineering. To evaluate the potential of NatureLM in generating materials with high bulk modulus, we conducted a detailed analysis of the generated compositions targeted at a bulk modulus of 400 GPa. From the generated outputs, we manually identified cases where MatterSim [77] predicted bulk modulus values within a 5 GPa range of the target. Two such cases were selected for further validation using density functional theory (DFT) calculations (see Fig. 17). The DFT results revealed bulk modulus values of 390 GPa and 394 GPa, which closely align with the target value of 400 GPa.

Beyond achieving the bulk modulus target, the two generated structures were confirmed to be novel compared to those available in the Materials Project database. This novelty underscores NatureLM’s potential for discovering new materials with exceptional mechanical properties, thereby broadening the scope of material design and innovation.

5.4 NatureLM-Mat3D: a crystal structure predictor for materials

Crystal material structure prediction (CSP) is a critical problem. Previous works apply random search, particle swarm algorithm, and a few others search

algorithms to look for stable crystal structures. More recently, generative models like VAE [78], diffusion [79] and flow matching based methods [80] are applied for such 3D structure generation. There is also a growing trend towards using Large Language Models (LLMs) for crystal structure generation, which can autoregressively generate the structures [80–82]. We fine-tune NatureLM to act as a crystal structure prediction module that generates 3D structures in an autoregressive manner.

Using NatureLM for structure prediction is particularly meaningful because it aligns the sequential modeling capacity of LLMs with the sequential representation of crystal structures. This congruence allows the model to capture the intricate dependencies and patterns inherent in material structures, potentially leading to more accurate and efficient generation of stable crystal configurations.

We represent materials and their 3D structures as 1D sequences in three steps:

1. *Flatten the chemical formula*: Repeat each element according to its count (e.g., A2B3 becomes A A B B B).
2. *Add space group information*: Append special tokens $\langle \text{sg} \rangle$ and $\langle \text{sgN} \rangle$, where N is the space group number.
3. *Include coordinate information*: Use the token $\langle \text{coord} \rangle$ to indicate the start of coordinates. Flatten the lattice parameters into nine float numbers and the fractional atomic coordinates into sequences of float numbers. Numbers are retained to four decimal places and tokenized character-wise (e.g., -3.1416 as - 3 . 1 4 1 6).

For example, the sequence for a material A2B3 with space group number 123 is:

A A B B B $\langle \text{sg} \rangle$ $\langle \text{sg123} \rangle$ $\langle \text{coord} \rangle$ 9 float numbers for lattice 15 float numbers for atoms

We collect data from Materials Project [83], NOMAD [84] and OQMD [85, 86] as our training data which are widely used database for materials with structure information, and test on MP-20, Perov-5 and MPTS-52 following previous works [78, 80, 87]. Specially, we remove duplications in the merged training data and remove all the data that appear in the test set in these benchmarks. The final training data contains about 6.5M samples after deduplication and removal of the test set. After training, we also finetuned the model on the training set for each benchmark to mitigate the different distributions between our training data and the benchmark data. We evaluate the match rate of the generated material structures and compare to CDVAE [78], DiffCSP [87] and FlowMM [80]. The results are shown in Table 15. Experiment results show that our sequence based auto-regressive method achieves comparable or best performance on MP-20 and MPTS-52 compared to other methods. We will use this for material structure generation in our following experiments. In future work, we will leverage and combine with more advanced methods like MatterGen [79] for structure generation.

	Perov-5		MP-20		MPTS-52	
	MR (%)	RMSE	MR (%)	RMSE	MR (%)	RMSE
CDVAE	45.31	0.1138	33.90	0.1045	5.34	0.2106
DiffCSP	52.02	0.0760	51.49	0.0631	12.19	0.1786
FlowMM	53.15	0.0992	61.39	0.0566	17.54	0.1726
NatureLM-Mat3D (1B)	50.78	0.0856	61.78	0.0436	30.20	0.0837

Table 15: The match rate (MR) and RMSE on Perov-5, MP-20 and MPTS-52.

NatureLM-Mat3D (1B) achieves performance that is comparable to or surpasses other state-of-the-art methods. The high match rates and low RMSE values demonstrate that our model effectively captures the complex spatial arrangements of atoms in crystal structures. Moreover we can see that NatureLM-Mat3D performs better than other methods as the number of atoms increases, demonstrating the advantage of autoregressive sequence model. As a next step, we plan to further improve the structure prediction quality by incorporating 3D autoregressive data into the pre-training phase of the next version of NatureLM.

6 Nucleotide tasks

The genome contains a vast amount of information regarding protein-coding genes and the regulatory DNA and RNA sequences that control their expression. In this section, we evaluated our model on nucleotide sequence generation tasks, including both unconditional generation and cross-domain generation, specifically DNA to RNA generation (guide RNA design) and protein to RNA generation.

6.1 Unconditional RNA generation

Designing RNA molecules is crucial for advancing RNA vaccines, nucleic acid therapies, and various biotechnological applications. In this section, we evaluate the proficiency of NatureLM in generating RNA sequences without any conditional prompts. For evaluation purposes, we constrained the generated RNA sequences to a maximum length of 1024 nucleotides. An example of an unconditionally generated sequence is provided below:

Instruction: `<rna>`
Response: `<rna> C C A C G G A G C C </rna>`

We assessed the quality of the generated RNA sequences by calculating their Minimum Free Energy (MFE) using RNAfold [88] (see Section C.2 for details). A lower MFE value indicates a potentially more stable RNA secondary structure. For each model, we generated 5,000 sequences and computed their MFE values. To establish a baseline for comparison, we generated control sequences and computed their average MFE values. Specifically, for each generated sequence, we created:

- (1) *Shuffled Sequences*: For each generated sequence, we created a new sequence by randomly shuffling its nucleotides, thereby preserving the original nucleotide composition and length but potentially disrupting any inherent structural motifs.
- (2) *Random Sequences*: For each generated sequence, we created an entirely random sequence of the same length, where each nucleotide position was independently sampled from the four nucleotides (A, G, C, U) with equal probability. This baseline represents sequences with no designed structure or composition bias.

As a reference for the MFE values of natural RNA sequences, we randomly sampled 5,000 sequences of length up to 1,024 nucleotides from RNACentral¹⁰ and computed their MFE values.

The average MFE values are reported in Table 16.

From the results, we observe that larger models tend to generate RNA sequences with lower (more negative) MFE values, indicating potentially more stable secondary structures. Additionally, shuffling and randomizing the

¹⁰<https://rnacentral.org/>

	MFE (kcal/mol)	Retrieved Rfam Families
RNAcentral	-165.4	
Shuffled sequences	-156.4	
Random sequences	-142.0	
NatureLM (1B)	-160.6	23
NatureLM (8B)	-170.6	38
NatureLM (8x7B)	-177.1	165

Table 16: Average MFE values (in kcal/mol) of RNA sequences generated by different methods and the number of unique Rfam families retrieved by different models. **MFE** denotes the mean Minimum Free Energy of the sequences. **Retrieved Rfam Families** represents the count of unique RNA families identified in the generated sequences using `cmscan`.

sequences result in higher (less negative) MFE values, suggesting that the original sequences generated by our models have structural features that contribute to stability.

To evaluate the diversity of the RNA sequences generated by NatureLM, we compared them to known RNA families in Rfam [89]. We used `cmscan` from the Infernal toolkit [90] to search for structural similarities between our generated sequences and the Rfam database (see Section C.2 for details). As shown in Table 16, larger models retrieved a significantly higher number of unique Rfam families than smaller models: the 1B, 8B, and 8x7B models retrieved 23, 38, and 165 unique families, respectively, covering a wider range of RNA functions. These results suggest that larger models not only generate more stable sequences but also encompass a more diverse set of RNA structures and functions.

6.2 Guide RNA design

Guide RNA (gRNA) plays a critical role in CRISPR-Cas9 gene editing by directing the Cas9 nuclease to a specific genomic target site. A gRNA consists of two components: a crRNA (crRNA), which is approximately 20 nucleotides long and complementary to the target DNA sequence, and a tracrRNA, which binds to Cas9. The crRNA garners more attention as it features a variable sequence critical for targeting specific DNA, whereas the tracrRNA has a more fixed role, primarily aiding in Cas9 binding. We evaluate NatureLM on two gRNA design tasks: the first is designing crRNA for a given DNA sequence, and the second is selecting the more effective crRNA from two candidates. Examples are provided below:

▷gRNA generation

Instruction:

Generate a guide RNA for targeting the DNA sequence
`<dna>GACTGGCACCAG...CCCTCGC</dna>`.

Response: `<rna>AGACACAGCGGGTGCTCTGC</rna>`

▷ More effective gRNA identification

Instruction: Investigate which of `<rna>ATGTAGAAGAATCCACCATA</rna>` or `<rna>GGAAGGGGTCAATATTCTCA</rna>` results in better wild-type efficiency for the DNA sequence `<dna>AAGGGGTGGCA...AGTGC</dna>`.

Response: `<rna>ATGTAGAAGAATCCACCATA</rna>`

For the first task of designing crRNA, the NatureLM’s identifies a targeted DNA region that includes the PAM sequence (Protospacer Adjacent Motif). To obtain the final crRNA, remove the ’NGG’ PAM sequence, reverse complement the DNA sequence, and apply the central dogma principle by converting DNA into RNA (replacing all ’T’ with ’U’). These quick and easy steps ensure the resulting crRNA is ready for use. A valid crRNA must meet the following criteria: (1) Be 17 to 24 nucleotides long. (2) Match a specific region in the provided DNA sequence. (3) Be followed by an ”NGG” Protospacer Adjacent Motif (PAM) in the DNA sequence, where ”N” represents any of the four standard nucleotide bases: adenine (A), cytosine (C), guanine (G), or thymine (T).

The example demonstrates that NatureLM accurately identifies the target sequence for guide RNA, ensuring the resulting guide RNA meets all necessary criteria—with an impressive accuracy of 95.7% in designing valid gRNAs.

NatureLM demonstrates a strong ability to generate valid gRNA sequences compared with generalist models like GPT4, accurately targeting the specified DNA while maintaining the PAM sequence feature. Furthermore, NatureLM shows proficiency in assessing the effectiveness of gRNAs, enabling it to select the more efficient gRNA from a given pair (Table 17).

Model	Validity	Top 1 accuracy
GPT-4	0.272	0.597
Llama 3 8B	0	0.38
Mixtral 8x7B	0	0.46
NatureLM (1B)	0.95	0.681
NatureLM (8B)	0.765	0.657
NatureLM (8x7B)	0.957	0.699

Table 17: The performance of guide RNA design.

6.3 Protein binding RNA design

RNA-binding proteins (RBPs) represent a large and diverse class of over 2,000 proteins that play a crucial role in regulating gene expression by interacting with RNA. Designing RNA decoys offers a powerful strategy to manipulate

these interactions. Such decoys can sequester RBPs away from their natural RNA targets, act as competitors to displace natural RNA molecules from RBPs, or serve as scaffolds to recruit RBPs to specific RNA molecules or cellular locations.

Instructions: Given `<protein>MSEY...SSGWGM</protein>`, create an RNA molecule that binds to it.

Response: `<rna>AAACAGG...CGTACGACA</rna>`

We selected 200 targets and generated binding RNA for them. To evaluate the generation ability of NatureLM, following [91], we trained a predictor for each protein to predict the binding affinity between the RNA and the protein. Specifically, the final layer of the classifier is a sigmoid function, which produces an output value ranging from 0 to 1, indicating the strength of the RNA-protein binding. If the score is greater than 0.5, we consider the generated RNA to have successfully bound to the protein.

We compared the RNA sequences generated by NatureLM 1B, 8B and 8x7B. Additionally, we used the predictors to evaluate the binding and non-binding RNA sequences from the test set. We also randomly selected RNA sequences of the same sizes from the unconditional generation setting for prediction (Section 6.1).

The results are summarized in Table 18, which reports the average and median prediction scores, as well as the success rate—the proportion of sequences with a prediction score above 0.5. We have the following observations:

1. As expected, binding RNA sequences achieved the highest average prediction score of 0.714 and a success rate of 74.5%, while the non-binding RNA sequences had the lowest average score of 0.274 and a success rate of 24.4%. This confirms the reliability of the classifiers and serving as a benchmark for optimal performance.
2. For unconditioned RNA Sequences, with an average score of 0.391 and a success rate of 36.3%, these sequences performed better than non-binding sequences but significantly worse than the binding sequences. This suggests that random RNA sequences have a moderate chance of being predicted as binders due to the intrinsic properties of RNA but lack the specificity achieved through conditioning.
3. For NatureLM generated sequences, as we increase the model sizes, there is a clear trend that larger models perform better. The results also demonstrated that NatureLM is more likely to generate RNA sequences that are likely to bind to the specified proteins when explicitly conditioned on them.

Source	AVG Score	Success rate (%)
Binding	0.714	74.5
Non-binding	0.274	24.4
Unconditioned	0.391	36.3
NatureLM (1B)	0.415	40.9
NatureLM (8B)	0.434	44.2
NatureLM (8x7B)	0.438	44.8

Table 18: Performance of designing protein-binding RNA given proteins: “AVG Scores” refers to the average prediction scores across all sequences. Success ratio refers to the percentage of scores that are greater than 0.5. See Figure [S15](#) for the detailed distribution of the predicted scores.

7 Prediction tasks

In addition to the generation and design tasks studied in previous sections, we also studied the predictive capabilities of NatureLM.

7.1 Small molecule prediction tasks

We evaluated NatureLM on three molecular property prediction tasks from MoleculeNet [92]: (i) predicting whether a molecule can cross the blood-brain barrier (BBBP); (ii) predicting whether a molecule can bind to the BACE receptor (BACE); (iii) predicting the toxicity of a molecule associated with 12 targets (Tox21). An illustrative example is presented below:

Instruction:

Can C1(c2ccccc2)=CCN(C)CC1 traverse the blood-brain barrier?

Response:

Yes.

Instruction:

Could the compound N(O)=C1CCC([NH2+]CC(O)C(Cc2cc(F)cc(F)c2)NC(C)=O)(c2ccccc(C(C)(C)C)c2)CC1 potentially restrain beta-secretase 1?

Response:

Yes.

To determine the probability of a “Yes” or “No” response, we first extract the probabilities output by the NatureLM, denoting the probability of “Yes” as p_1 and the probability of “No” as p_2 . We then normalized these probabilities: the probability of “Yes” is calculated as $p_1/(p_1 + p_2)$ while the probability of “No” is $p_2/(p_1 + p_2)$.

All tasks in this subsection are measured by AUROC¹¹. The results are reported in Table 19. Generally, larger models achieve better performance, while there is still a gap between the current NatureLM and the state-of-the-art specialist models.

	BBBP	Bace	Tox21
DVMP [93]	78.1	89.3	78.8
BioT5 [56]	77.7	89.4	77.9
NatureLM (1B)	71.1	79.4	68.3
NatureLM (8B)	70.2	82.0	69.8
NatureLM (8x7B)	73.7	83.1	72.0

Table 19: Molecular property prediction on MoleculeNet [92]. The evaluation metric is the AUROC score.

¹¹https://scikit-learn.org/1.5/modules/generated/sklearn.metrics.roc_auc_score.html

7.2 Protein prediction tasks

We evaluated the NatureLM on four protein property classification tasks, including solubility prediction, stability prediction, and protein-protein interaction (PPI) prediction for both human and yeast proteins. These datasets as well as the data splits are adopted from the PEER benchmark [94]. An example is provided below:

Instruction:

Does the sequence of this protein suggest it would be stable? Please answer ‘Yes’ if it is stable and ‘No’ if it is not. `<protein>TTIKVNG ...KVTR</protein>`

Response:

No.

Instruction: Could these proteins interact, considering their sequences? The first protein is

`<protein>MPPS ...VETVV</protein>`, the second protein is `<protein>MSLHF ...PLGCCR</protein>`. Please respond with ‘Yes’ if the proteins can interact and ‘No’ if they cannot.

Response:

Yes

Model Setting	Solubility	Stability	Human PPI	Yeast PPI
Literature SOTA	0.702	-	0.881	0.661
SFM-Protein (650M) [69]	0.744	0.583	0.852	0.628
NatureLM (1B)	0.684	0.682	0.781	0.561
NatureLM (8B)	0.714	0.635	0.848	0.604
NatureLM (8x7B)	0.698	0.723	0.776	0.586

Table 20: Protein understanding task comparison (accuracy). Please note that the NatureLM models are trained for various diverse tasks in a unified way and evaluated separately on these tasks by the same model, while the state-of-the-art models are trained and tested individually for each task.

Table 20 presents the accuracy of our models on various protein understanding tasks. Overall, the results highlight that our unified NatureLM models perform competitively with task-specific models, even surpassing them in certain tasks like stability prediction. This demonstrates the effectiveness of our training strategy, where a single model can learn and generalize across diverse protein understanding tasks without the need for separate models for each task.

7.3 DNA prediction tasks

We selected two classification tasks to assess the model’s capability of identifying significant sequence motifs implicated in human gene regulation. These tasks include the identification of promoters and transcription factor binding sites. We utilized datasets from the Genome Understanding Evaluation (GUE, see Appendix B.2 of [18] for a summary), converting them into a format suitable for instruction tuning. An example is shown below:

<p>Instruction: Verify if there is a promoter region within <dna>TGGACT··TGAGCTC</dna>?</p> <p>Response: Yes.</p> <p>Instruction: Can the sequence <dna>GCCTGCCAG··AAAAC</dna> be classified as a transcription factor binding site?</p> <p>Response: No.</p>

Model	Promoter detection	Core promoter detection	TF binding
NT-2500M-multi [95]	0.881	0.716	0.633
DNABERT2 [96]	0.842	0.705	0.701
NatureLM (1B)	0.805	0.571	0.524
NatureLM (8B)	0.827	0.595	0.549
NatureLM (8x7B)	0.835	0.602	0.560

Table 21: Performance comparison of various models on DNA property prediction tasks, evaluated using Matthews Correlation Coefficient (MCC).

Table 21 presents the results of our experiments, evaluated using the Matthews Correlation Coefficient (MCC). For the Transcription Factor Binding prediction task, we conducted separate predictions on specific ChIP-seq datasets: POLR2A ChIP-seq on human HUVEC, POLR2A ChIP-seq on human ProgFib, PAX5 ChIP-seq protocol v041610.1 on human GM12892, TRIM28 ChIP-seq on human U2OS, and MXI1 ChIP-seq on human H1-hESC produced by the Snyder lab. We then calculated the average performance across these datasets. Despite a performance gap between our models and the state-of-the-art, the observed improvements with increasing model sizes suggest potential for further advancements. These findings indicate that larger models may more effectively capture the complex regulatory motifs involved in human gene regulation.

8 Strategies to further improve performance

In this section, we examine two strategies to improve the model’s performance: reinforcement learning for scenarios with limited labeled data for fine-tuning specific tasks, and dedicated fine-tuning for cases where sufficient labeled data is available for particular tasks.

8.1 Reinforcement enhanced NatureLM

Reinforcement Learning with Human Feedback (RLHF) is well-established approach to enhance foundation models. This section explores how to utilize preference signals in RLHF, moving beyond reliance on direct supervised signals¹². For many generative tasks, where answers are open-ended and do not have a single correct solution, training with preference signals offers a more intuitive approach.

For RLHF training, we curated preference data from nine property optimization tasks related to small molecules: BBBP, BACE, LogP, Donor, QED, CYP1A2, CYP2C9, CYP2D6, and CYP3A4. Detailed descriptions of each task and the corresponding data quantities can be found in Table S6. In total, we compiled 179.5k data points. Note that we used all the data to enhance the post-trained NatureLM (8B), resulting in a single model for the nine tasks after RLHF.

The data is structured in a preference-based format, where each sample consists of a prompt, along with both an accepted and a rejected response. An example of this format is presented below:

Instruction:

Enhance the effectiveness of the molecule

<mol>COc1cc2c(c(OC)c1OC)-c1ccc(OC)c(=O)cc1[C@@H](NC(C)=O)CC2</mol> in penetrating the blood-brain barrier.

Accepted Response:

<mol>COc1cc2c(c(OC)c1OC)-c1ccc(OC)c(=O)cc1C(NC(C)=O)CC2</mol>

Reject Response:

<mol>COc1cc2c(c(OC)c1OC)-c1ccc(OC)c(=O)cc1[C@@H](NC(C)=O)CC2</mol>

In the example above, the compound in the accepted response is capable of crossing the BBB, whereas the compounds in the instruction and rejected response cannot.

We leveraged Direct Preference Optimization (DPO) [97] to enhance the molecule optimization ability of NatureLM. The loss of DPO algorithm is written as follows:

¹²It is important to note that direct signals have already been used in post-training (see Section 2.5).

$$\mathcal{L}_{\text{DPO}}(\pi_{\theta}; \pi_{\text{ref}}) = -\mathbb{E}_{(x, y_w, y_l) \sim \mathcal{D}} \left[\log \sigma \left(\beta \log \frac{\pi_{\theta}(y_w | x)}{\pi_{\text{ref}}(y_w | x)} - \beta \log \frac{\pi_{\theta}(y_l | x)}{\pi_{\text{ref}}(y_l | x)} \right) \right], \quad (3)$$

where π_{ref} is the model after post-training and fixed during DPO training, π_{θ} is the model to optimize and set to π_{ref} before DPO training, x is the prompt, y_w is the accepted response, y_l is the reject response, and β is a hyper-parameter.

Property	Δ
QED	0.6
LogP	0.6
Donor	0.6
BBBP	2.9
BACE	3.5
CYP1A2	2.3
CYP2C9	0.7
CYP2D6	0.7
CYP3A4	1.0

Table 22: Results of the reinforcement optimization. Let r_1 and r_2 represent the outcomes before and after applying reinforcement, respectively, and let Δ denote the percentage improvement, i.e., $\Delta = (r_2 - r_1)/r_1 \times 100\%$.

Table 22 shows the improvements of DPO training over the 9 property optimization tasks. Notably, the model had already undergone instruction tuning (the post-training in Section 3) prior to DPO training, and no new data was introduced during the DPO process. The results highlight how reformatting the data into a preference-based structure allows the DPO algorithm to improve performance across multiple tasks simultaneously.

Looking ahead, we plan to generate data on the fly in RLHF and utilize additional reward models to evaluate the properties of newly generated molecules, thereby creating better preference-based data.

8.2 Dedicated fine-tuning on retrosynthesis

We dedicatedly fine-tuned our NatureLM model to evaluate its performance against specialized models in the retrosynthesis prediction task, using a large-scale labeled dataset, the Pistachio reaction dataset [98], with 15 million reactions from U.S., European, and WIPO patents. To ensure data quality, we removed any invalid or duplicate reactions. The cleaned dataset was then randomly split into a training set with 3.1 million reactions and a test set with 34,000 reactions.

Before training, we preprocessed the input products and output reactants using a root-aligned SMILES format [65]. This format offers a clear one-to-one mapping between the product and reactant SMILES, thereby enhancing

prediction efficiency. Additionally, we augmented the training dataset tenfold to further improve the model’s performance. As shown in Table 23, NatureLM (1B) demonstrates competitive performance, rivaling leading template-based models (e.g., LocalRetro) and template-free models (e.g., R-SMILES) on the large Pistachio dataset.

	Top-1 accuracy	Top-3 accuracy
LocalRetro [64]	40.8%	56.6%
R-SMILES [65]	51.2%	67.1%
NatureLM (1B)	51.4%	66.0%

Table 23: Retrosynthesis prediction results on Pistachio dataset.

8.3 Dedicated fine-tuning on Matbench

We fine-tuned our NatureLM 8B model on Matbench [99], a benchmark for state-of-the-art machine learning algorithms that predict various properties of solid materials. Matbench is hosted and maintained by the Materials Project [83]. Following the approach in [100], we fine-tuned a single model for three tasks from Matbench, rather than developing separate models for each task.

The results are presented in Table 24 to 26. Results of baseline models are collected from the official leader board¹³. As can be seen, NatureLM achieves state-of-the-art performance on matbench_expt_gap and matbench_is_metal.

Model	MAE ↓	Model	F1 ↑	Model	F1 ↑
Dummy[99]	1.1435	Dummy[99]	0.4913	Dummy[99]	0.7127
gptchem[101]	0.4544	gptchem[101]	0.8953	DARWIN[100]	0.8722
RF-SCM/ Magpie[99]	0.4461	MODNet[102]	0.9153	gptchem[101]	0.8782
AMMExpress[99]	0.4161	RF-SCM/ Magpie[99]	0.9159	Magpie[99]	0.9278
MODNet[102]	0.3327	AMMExpress[99]	0.9200	AMMExpress[99]	0.9043
Ax/SAASBO	0.3310	DARWIN[100]	0.9599	MODNet[102]	0.9784
CrabNet[103, 104]					
DARWIN[100]	0.2865	NatureLM	0.9630	NatureLM	0.8720
NatureLM	0.2858				

Table 24: Results on matbench_expt_gap.

Table 25: Results on matbench_is_metal.

Table 26: Results on matbench_glass.

¹³<https://matbench.materialsproject.org/>

9 Text capabilities

We assess the text-related capabilities of NatureLM (8x7B) in this section. We first present several examples to provide readers with an intuitive understanding (Section 9.1), and then benchmark results from AlpacaEval (Section 9.2).

9.1 Case study

Here we demonstrate our model’s language capabilities in scientific discovery research. Specifically, we assessed the model’s understanding of CRISPR gene editing, cancer immunotherapy, and drug discovery. A few selected cases are presented in this section for brevity. Additional cases can be found in Fig. S17, S18 and S19.

9.1.1 CRISPR gene editing

CRISPR gene editing has rapidly emerged as a powerful tool in biotechnology. Our model demonstrates a good understanding of CRISPR and is able to effectively analyze the advantages and disadvantages of commonly used CRISPR tools.

Instruction: Could you provide me the advantages and disadvantages of Cas9?

Response:

Advantages: 1. Highly efficient and specific gene editing with a low risk of off-target effects. 2. Can target a wide range of sequences. 3. Can be used to make specific alterations to genes in virtually any organism. Disadvantages: 1. Potential for off-target effects when using Cas9. 2. The delivery of Cas9 can be inefficient. 3. Lack of control over the repair mechanism. 4. May cause chromosomal abnormalities.

Instruction: Could you provide me the advantages and disadvantages of Cas12a, another widely used CRISPR protein?

Response:

Advantages:

1. High specificity: Cas12a has higher specificity compared to Cas 9, which reduces off-target effects. 2. Simpler PAM requirements: Cas 12a requires a simpler PAM sequence than Cas9, making it easier to target specific genomic loci. 3. Multiplexing: Cas12a can be used for multiplexing genome editing, meaning multiple genomic loci can be edited in a single reaction. Disadvantages:

4. Lower efficiency: Cas12a is less efficient in terms of indel formation than Cas9. 5. Larger size: Cas12a is a larger protein than Cas9, which can make it harder to deliver the Cas12a system into cells.

...

Fig. 18: Cases about CRISPR gene editing.

9.1.2 Cancer immunotherapy

Our model is knowledgeable about existing checkpoint inhibitors used in cancer therapy and provides accurate explanations of their mechanisms of action. Specifically, in our experiment, it generates a valid peptide sequence for inhibiting the overexpressed PD-L1 protein (see Figure S18), although the length of the peptide is incorrect. It demonstrates a solid understanding of the inhibition cascade between drugs and proteins.

Instruction: Tell me existing checkpoint inhibitors for PD-L1.

Response: The checkpoint inhibitors for PD-L1 that are currently approved by the FDA include atezolizumab, avelumab, duravalumab, and perbrolizumab.

Instruction: PD-L1 is a protein that inhibits PD-1, a receptor found on T cells. This new drug X, is designed to inhibit PD-L1. If we introduce drug X, will T cell function be restored? Explain it step by step.

Response: PD-1 is inhibited by interaction with PD-L1. If drug X inhibits PD-L1, PD-1 will no longer be inhibited. Therefore, T cell function will be restored. Therefore, the answer is yes.

Fig. 19: Cases about cancer immunotherapy.

9.1.3 Drug discovery

Drug discovery is an evolving process that incorporates empirical rules, computational design, and experimental validation. The model demonstrates an understanding of the fundamental principles of drug discovery. Specifically, when being asked questions about Lipinski's Rule of Five and strategies (see Figure S19) to improve a drug's ADME properties, the model provides mostly accurate answers.

Instruction: What approaches can drug experts use to enhance a drug's ADME properties?

Response: Structure-based drug design: Computational techniques can be used to modify existing drugs or design new ones with desired ADME properties. 2. Lipophilicity: Lipophilicity can affect the ADME profile of a drug. 3. Hepatic and extracellular clearance: Understanding the hepatic and extracellular clearance of a drug is important for assessing its ADME profile. 4. Microsomal stability: Microsomal stability is a measure of how quickly a drug is broken down by liver enzymes. 5. Oral absorption: Oral absorption is determined by the solubility and permeability of a drug. 6. Permeability: The ability of a drug to cross cell membranes affects its bioavailability. ...

Fig. 20: Case about drug discovery.

9.2 Comparison on AlpacaEval evaluation

To assess the linguistic capabilities of NatureLM, we compared NatureLM (8x7B) with the original Mixtral (8x7B) using the AlpacaEval [105] dataset and method. AlpacaEval is a benchmark for LLM designed to gauge a model’s proficiency in executing general user instructions. NatureLM’s responses are compared against reference responses generated by original Mixtral using GPT-4 as the annotator. We focused on two metrics from AlpacaEval: the general win rate and the LC win rate (length-controlled win rate), which controls the bias introduced by the length of the responses. Our NatureLM model achieved a LC win rate of 31.8% and a win rate of 25.2% when benchmarked against Mixtral, showcasing that while the model possesses a foundational level of language comprehension, it exhibits constraints in its linguistic capacity. A potential contributing factor to this limited performance is the overrepresentation of scientific data within the training dataset, which may skew the model’s proficiency towards technical language and away from a more generalized understanding required for diverse user instructions. Fig. S20 presents two illustrative examples from the AlpacaEval comparison. We will improve the text capabilities of NatureLM in our future work.

10 Ablation study

To better understand the contributions of different components in our model and training process, we conducted ablation studies focusing on two aspects: (1) the impact of including general text-based instruction tuning data in post-training, and (2) the effectiveness of continuing pretraining on scientific data before post-training, as opposed to directly fine-tuning from the baseline model. We evaluated the results across 7 tasks, including four small molecule tasks (Molecular property prediction, IUPAC to SMILES translation, Retrosynthesis, Metabolism optimization), two protein tasks (Protein description generation, CDR-H3 generation) and two DNA tasks (DNA property prediction). The results are reported in Fig. 21.



Fig. 21: Ablation study results. NatureLM models are denoted as “(w/ text)”. The NatureLM models without text instruction data for post-training are denoted as “(w/o text)”. Additionally, we fine-tuned the original Llama 3 model, denoted as “Llama 3 8B (w/ text)”. Performance metrics are displayed in the cells (larger values indicate better performance), with rank represented by the color intensity (darker colors signify higher rankings).

10.1 Impact of text-based post-training data

We investigated whether incorporating general text instruction tuning data into the post-training phase affects the performance of NatureLM. To this end, we compared the results of NatureLM post-trained with or without the inclusion of general text-based instruction data during the post-training phase. NatureLM (1B w/o text) and NatureLM (8B w/o text) denote the models without text data for post-training. We have several observations from Fig. 21:

- For the 1B parameter models, post-training without general text-based instruction data leads to better performance on scientific tasks, as evidenced by the superior performance on 5 out of 8 tasks. This suggests that at smaller scales, including text-based instruction data may not provide benefits and could potentially dilute the model’s focus on scientific instructions due to limited model capacity.
- In contrast, for the 8B parameter models, post-training with text-based instruction data does not adversely affect performance. This indicates that the larger model has sufficient capacity to incorporate both general text-based and science-based instruction data without detrimental effects on its performance on scientific tasks.

10.2 Impact of continued pre-training on scientific data

One might wonder whether it is necessary to pre-train a foundation model on scientific data or if directly fine-tuning a large language model (LLM) with scientific instruction data suffices. To address these questions, we compared our NatureLM (8B) model, which initially continues pre-training of Llama 3 8B on scientific data before undergoing post-training with scientific instruction data, against a model that directly fine-tunes the Llama 3 8B model without the pre-training step. As shown in Fig. 21, NatureLM (8B) outperforms the directly fine-tuned Llama 3 8B across all tasks, highlighting the importance of pre-training on a scientific corpus.

11 Discussions

11.1 Summary

In this work, we developed Nature Language Model (NatureLM), a sequence-based science foundation model for scientific discovery across multiple domains. Users can interact with the model using text-based instructions to generate novel scientific entities. It supports cross-domain generation and has been demonstrated in phases of drug discovery, protein generation, RNA generation, and enables predictive capabilities for small molecules, proteins, and DNA. Among the 22 tasks tested, larger models showed better performance on 18 tasks. We believe NatureLM is a significant step towards transforming scientific discovery with foundation model approaches.

11.2 Limitations

Despite the progress of NatureLM, we have identified several limitations and are committed to addressing them in future versions:

Language Capabilities: Interacting with scientific models using human language will be an essential feature to enable scientific discoveries. Although NatureLM demonstrates general language capabilities, it achieves only a 31.8% winning rate on the AlpacaEval benchmark when compared to the original Mixtral

8x7B. To enhance this, we plan to incorporate more high-quality text data in pre-training in the future.

Few-shot Capabilities: The capability of few-shot learning is critical for a foundation model. Currently, our NatureLM does not exhibit strong few-shot capabilities. We aim to enhance this by refining our training strategies and increasing the model size.

11.3 Cross-domain applications

NatureLM is a unified model that spans multiple domains, including text, small molecules, proteins, materials, and nucleotides. One significant advantage of this multi-domain unification is that it allows for the integration of knowledge from diverse fields, enabling us to tackle important cross-domain tasks that domain-specific models cannot address. While we have already provided a few examples of cross-domain tasks, here are several more that we plan to study in the future:

1. *Design of Biocompatible Materials:* Developing biocompatible materials requires the simultaneous consideration of material properties and protein interactions. Examples included the Titanium Alloys and Cobalt-Chromium Alloys used in hip replacement.
2. *Ribozyme and Bio-Catalyst Development:* Designing effective ribozymes and bio-catalysts necessitates a detailed understanding of RNA structures, protein functions, and small molecule interactions.
3. *Enabling Complex System Understanding:* Systems biology aims to understand the complex interplay of various components in a system, including biomolecules such as proteins, DNA, RNA, lipids, carbohydrates, and small molecules like metabolites.

Author list

Yingce Xia*, Peiran Jin*, Shufang Xie*, Liang He*, Chuan Cao*, Renqian Luo*, Guoqing Liu*, Yue Wang*, Zequn Liu*, Yuan-Jyue Chen*, Zekun Guo*, Yeqi Bai, Pan Deng, Yaosen Min, Ziheng Lu, Hongxia Hao, Han Yang, Jielan Li, Chang Liu, Jia Zhang, Jianwei Zhu, Ran Bi, Kehan Wu, Wei Zhang, Kaiyuan Gao, Qizhi Pei, Qian Wang, Xixian Liu, Yanting Li, Houtian Zhu, Yeqing Lu, Mingqian Ma, Zun Wang, Tian Xie, Krzysztof Maziarz, Marwin Segler, Zhao Yang, Zilong Chen, Yu Shi, Shuxin Zheng, Lijun Wu, Chen Hu, Peggy Dai, Tie-Yan Liu, Haiguang Liu, Tao Qin

* indicates co-first authors.

Corresponding authors: Tao Qin and Yingce Xia

Contact emails: {taoqin, yingce.xia}@microsoft.com

This work was conducted in Microsoft Research AI for Science.

Acknowledgements

We extend our gratitude to Dr. Fan Yang and Dr. Jilong Xue for their support with large-scale model training. We thank Likun Dong and Junren Li for conducting the case study on retrosynthesis and the SMILES-to-IUPAC translation. Our thanks also go to Dr. Claudio Zeni, Dr. Robert Pinsler, Dr. Daniel Zügner, Dr. Andrew Fowler, Dr. Matthew Horton, and Dr. Ryota Tomioka for their assistance with material tasks. We appreciate the constructive feedback from Dr. Bichlien Nguyen, Dr. Jake Smith, and Dr. Frank Noé. We thank Dr. Han Guo for visualizing the molecules in our paper. We acknowledge Jingyun Bai for improving the quality of the figures. We thank Dr. Christopher Bishop for his invaluable guidance and sponsorship of this work.

This work was done when Zekun Guo, Kehan Wu, Wei Zhang, Kaiyuan Gao, Qizhi Pei, Qian Wang, Xixian Liu, Yanting Li, Houtian Zhu, Yeqing Lu, Mingqian Ma, Zhao Yang, Zilong Chen were interns at Microsoft Research AI for Science.

References

- [1] Brown, T.B., Mann, B., Ryder, N., et. al: Language Models are Few-Shot Learners (2020). <https://arxiv.org/abs/2005.14165>
- [2] OpenAI, Achiam, J., et. al: GPT-4 Technical Report (2024). <https://arxiv.org/abs/2303.08774>
- [3] OpenAI, Hurst, A., et. al.: GPT-4o System Card (2024). <https://arxiv.org/abs/2410.21276>
- [4] Team, G., Anil, R., et. al: Gemini: A Family of Highly Capable Multimodal Models (2024). <https://arxiv.org/abs/2312.11805>
- [5] Team, G., Georgiev, P., et. al.: Gemini 1.5: Unlocking multimodal understanding across millions of tokens of context (2024). <https://arxiv.org/abs/2403.05530>
- [6] Abdin, M., Aneja, J., Awadalla, H., et. al: Phi-3 Technical Report: A Highly Capable Language Model Locally on Your Phone (2024). <https://arxiv.org/abs/2404.14219>
- [7] Abdin, M., Aneja, J., Behl, H., et. al: Phi-4 Technical Report (2024). <https://www.microsoft.com/en-us/research/uploads/prod/2024/12/P4TechReport.pdf>
- [8] Llama Team, A.a.M.: The Llama 3 Herd of Models (2024). <https://arxiv.org/abs/2407.21783>
- [9] Jiang, A.Q., Sablayrolles, A., Mensch, A., Bamford, C., Chaplot, D.S., de las Casas, D., Bressand, F., Lengyel, G., Lample, G., Saulnier, L., Lavaud, L.R., Lachaux, M.-A., Stock, P., Scao, T.L., Lavril, T., Wang, T., Lacroix, T., Sayed, W.E.: Mistral 7B (2023). <https://arxiv.org/abs/2310.06825>
- [10] Jiang, A.Q., Sablayrolles, A., Roux, A., Mensch, A., Savary, B., Bamford, C., Chaplot, D.S., de las Casas, D., Hanna, E.B., Bressand, F., Lengyel, G., Bour, G., Lample, G., Lavaud, L.R., Saulnier, L., Lachaux, M.-A., Stock, P., Subramanian, S., Yang, S., Antoniak, S., Scao, T.L., Gervet, T., Lavril, T., Wang, T., Lacroix, T., Sayed, W.E.: Mixtral of Experts (2024). <https://arxiv.org/abs/2401.04088>
- [11] DeepSeek-AI, et. al: DeepSeek-V3 Technical Report (2024). <https://arxiv.org/abs/2412.19437>
- [12] DeepSeek-AI, et. al: DeepSeek-R1: Incentivizing Reasoning Capability in LLMs via Reinforcement Learning (2025). <https://arxiv.org/abs/2501.12948>

- [13] Yang, A., Yang, B., Hui, B., et. al: Qwen2 Technical Report (2024). <https://arxiv.org/abs/2407.10671>
- [14] Qwen, Yang, A., et. al: Qwen2.5 Technical Report (2025). <https://arxiv.org/abs/2412.15115>
- [15] AI4Science, M.R., Quantum, M.A.: The Impact of Large Language Models on Scientific Discovery: a Preliminary Study using GPT-4 (2023). <https://arxiv.org/abs/2311.07361>
- [16] Madani, A., Krause, B., Greene, E.R., Subramanian, S., Mohr, B.P., Holton, J.M., Olmos, J.L., Xiong, C., Sun, Z.Z., Socher, R., Fraser, J.S., Naik, N.: Large language models generate functional protein sequences across diverse families. *Nature Biotechnology* **41**(8), 1099–1106 (2023). <https://doi.org/10.1038/s41587-022-01618-2>
- [17] Hayes, T., Rao, R., Akin, H., Sofroniew, N.J., Oktay, D., Lin, Z., Verkuil, R., Tran, V.Q., Deaton, J., Wiggert, M., Badkundri, R., Shafkat, I., Gong, J., Derry, A., Molina, R.S., Thomas, N., Khan, Y., Mishra, C., Kim, C., Bartie, L.J., Nemeth, M., Hsu, P.D., Sercu, T., Candido, S., Rives, A.: Simulating 500 million years of evolution with a language model. *bioRxiv* (2024) <https://arxiv.org/abs/https://www.biorxiv.org/content/early/2024/07/02/2024.07.01.600583.full.pdf>. <https://doi.org/10.1101/2024.07.01.600583>
- [18] Zhou, Z., Ji, Y., Li, W., Dutta, P., Davuluri, R.V., Liu, H.: DNABERT-2: Efficient foundation model and benchmark for multi-species genomes. In: *The Twelfth International Conference on Learning Representations* (2024). <https://openreview.net/forum?id=oMLQB4EZE1>
- [19] Nguyen, E., Poli, M., Durrant, M.G., Kang, B., Katrekar, D., Li, D.B., Bartie, L.J., Thomas, A.W., King, S.H., Brix, G., Sullivan, J., Ng, M.Y., Lewis, A., Lou, A., Ermon, S., Baccus, S.A., Hernandez-Boussard, T., Ré, C., Hsu, P.D., Hie, B.L.: Sequence modeling and design from molecular to genome scale with evo. *Science* **386**(6723), 9336 (2024). <https://doi.org/10.1126/science.ado9336>
- [20] Cui, H., Wang, C., Maan, H., Pang, K., Luo, F., Duan, N., Wang, B.: scgpt: toward building a foundation model for single-cell multi-omics using generative ai. *Nature Methods* **21**(8), 1470–1480 (2024). <https://doi.org/10.1038/s41592-024-02201-0>
- [21] Liu, Z., Zhang, W., Xia, Y., Wu, L., Xie, S., Qin, T., Zhang, M., Liu, T.-Y.: Molxpt: Wrapping molecules with text for generative pre-training. In: *Proceedings of the 61st Annual Meeting of the Association for Computational Linguistics (Volume 2: Short Papers)*, pp. 1606–1616 (2023)

- [22] Segler, M.H., Kogej, T., Tyrchan, C., Waller, M.P.: Generating focused molecule libraries for drug discovery with recurrent neural networks. *ACS central science* **4**(1), 120–131 (2018)
- [23] Chaves, J.M.Z., Wang, E., Tu, T., Vaishnav, E.D., Lee, B., Mahdavi, S.S., Semturs, C., Fleet, D., Natarajan, V., Azizi, S.: Tx-llm: A large language model for therapeutics. arXiv preprint arXiv:2406.06316 (2024)
- [24] Lv, L., Lin, Z., Li, H., Liu, Y., Cui, J., Chen, C.Y.-C., Yuan, L., Tian, Y.: ProLLaMA: A Protein Language Model for Multi-Task Protein Language Processing (2024). <https://arxiv.org/abs/2402.16445>
- [25] Luo, R., Sun, L., Xia, Y., Qin, T., Zhang, S., Poon, H., Liu, T.-Y.: Biogpt: generative pre-trained transformer for biomedical text generation and mining. *Briefings in Bioinformatics* **23**(6), 409 (2022) <https://arxiv.org/abs/https://academic.oup.com/bib/article-pdf/23/6/bbac409/47144271/bbac409.pdf>. <https://doi.org/10.1093/bib/bbac409>
- [26] Taylor, R., Kardas, M., Cucurull, G., Scialom, T., Hartshorn, A., Saravia, E., Poulton, A., Kerkez, V., Stojnic, R.: Galactica: A Large Language Model for Science (2022). <https://arxiv.org/abs/2211.09085>
- [27] Liang, Y., Zhang, R., Zhang, L., Xie, P.: DrugChat: Towards Enabling ChatGPT-Like Capabilities on Drug Molecule Graphs (2023). <https://arxiv.org/abs/2309.03907>
- [28] Wang, C., Fan, H., Quan, R., Yang, Y.: ProtChatGPT: Towards Understanding Proteins with Large Language Models (2024). <https://arxiv.org/abs/2402.09649>
- [29] Weininger, D.: Smiles, a chemical language and information system. 1. introduction to methodology and encoding rules. *Journal of Chemical Information and Computer Sciences* **28**(1), 31–36 (1988). <https://doi.org/10.1021/ci00057a005>
- [30] Bond-Taylor, S., Leach, A., Long, Y., Willcocks, C.G.: Deep generative modelling: A comparative review of vaes, gans, normalizing flows, energy-based and autoregressive models. *IEEE transactions on pattern analysis and machine intelligence* **44**(11), 7327–7347 (2021)
- [31] Yenduri, G., Ramalingam, M., Selvi, G.C., Supriya, Y., Srivastava, G., Maddikunta, P.K.R., Raj, G.D., Jhaveri, R.H., Prabadevi, B., Wang, W., et al.: Gpt (generative pre-trained transformer)–a comprehensive review on enabling technologies, potential applications, emerging challenges, and future directions. *IEEE Access* (2024)

- [32] Landrum, G., Tosco, P., Kelley, B., Rodriguez, R., Cosgrove, D., Vianello, R., sriniker, Geddeck, P., Jones, G., NadineSchneider, Kawashima, E., Nealschneider, D., Dalke, A., Swain, M., Cole, B., Turk, S., Savelev, A., tadhurst-cdd, Vaucher, A., Wójcikowski, M., Take, I., Scalfani, V.F., Walker, R., Ujihara, K., Probst, D., Lehtivarjo, J., Faara, H., guillaume godin, Pahl, A., Monat, J.: Rdkit/rdkit: 2024_09_5 (Q3 2024) Release. <https://doi.org/10.5281/zenodo.14779836>
- [33] Wang, Y.-C., Yang, W.-H., Yang, C.-S., Hou, M.-H., Tsai, C.-L., Chou, Y.-Z., Hung, M.-C., Chen, Y.: Structural basis of SARS-CoV-2 main protease inhibition by a broad-spectrum anti-coronaviral drug. *Am. J. Cancer Res.* **10**(8), 2535–2545 (2020)
- [34] Davey, C.A., Sargent, D.F., Luger, K., Maeder, A.W., Richmond, T.J.: Solvent mediated interactions in the structure of the nucleosome core particle at 1.9Å resolution. *J. Mol. Biol.* **319**(5), 1097–1113 (2002)
- [35] Pettersen, E.F., Goddard, T.D., Huang, C.C., Couch, G.S., Greenblatt, D.M., Meng, E.C., Ferrin, T.E.: UCSF chimera—a visualization system for exploratory research and analysis. *J. Comput. Chem.* **25**(13), 1605–1612 (2004)
- [36] Materials Project, T.: Materials data on li2o by materials project (2020). <https://doi.org/10.17188/1194803>
- [37] Sung, M., Jeong, M., Choi, Y., Kim, D., Lee, J., Kang, J.: BERN2: an advanced neural biomedical named entity recognition and normalization tool. *Bioinformatics* **38**(20), 4837–4839 (2022) <https://arxiv.org/abs/https://academic.oup.com/bioinformatics/article-pdf/38/20/4837/46535173/btac598.pdf>. <https://doi.org/10.1093/bioinformatics/btac598>
- [38] Zhu, W., Hessel, J., Awadalla, A., Gadre, S.Y., Dodge, J., Fang, A., Yu, Y., Schmidt, L., Wang, W.Y., Choi, Y.: Multimodal c4: An open, billion-scale corpus of images interleaved with text. *ArXiv abs/2304.06939* (2023)
- [39] Zhan, J., Dai, J., Ye, J., Zhou, Y., Zhang, D., Liu, Z., Zhang, X., Yuan, R., Zhang, G., Li, L., Yan, H., Fu, J., Gui, T., Sun, T., Jiang, Y., Qiu, X.: Anygpt: Unified multimodal llm with discrete sequence modeling. *ArXiv abs/2402.12226* (2024)
- [40] Team, C.: Chameleon: Mixed-Modal Early-Fusion Foundation Models (2024)
- [41] Soboleva, D., Al-Khateeb, F., Myers, R., Steeves, J.R., Hestness,

- J., Dey, N.: SlimPajama: A 627B token cleaned and deduplicated version of RedPajama. <https://www.cerebras.net/blog/slimpajama-a-627b-token-cleaned-and-deduplicated-version-of-redpajama> (2023). <https://huggingface.co/datasets/cerebras/SlimPajama-627B>
- [42] Kwon, W., Li, Z., Zhuang, S., Sheng, Y., Zheng, L., Yu, C.H., Gonzalez, J., Zhang, H., Stoica, I.: Efficient memory management for large language model serving with pagedattention. In: Proceedings of the 29th Symposium on Operating Systems Principles, pp. 611–626 (2023)
- [43] Yu, G.-I., Jeong, J.S., Kim, G.-W., Kim, S., Chun, B.-G.: Orca: A distributed serving system for {Transformer-Based} generative models. In: 16th USENIX Symposium on Operating Systems Design and Implementation (OSDI 22), pp. 521–538 (2022)
- [44] vllm-project: vLLM: A high-throughput and memory-efficient inference and serving engine for LLMs. Accessed: 2024-10-15 (2024). <https://github.com/vllm-project/vllm>
- [45] Yu, B., Baker, F.N., Chen, Z., Ning, X., Sun, H.: Lllasmol: Advancing large language models for chemistry with a large-scale, comprehensive, high-quality instruction tuning dataset. arXiv preprint arXiv:2402.09391 (2024)
- [46] Anthropic: The claude 3 model family: Opus, sonnet, haiku (2024)
- [47] Rajan, K., Zielesny, A., Steinbeck, C.: Stout v2. 0: Smiles to iupac name conversion using transformer models (2024)
- [48] Xia, Y., Wu, K., Deng, P., Liu, R., Zhang, Y., Guo, H., Cui, Y., Pei, Q., Wu, L., Xie, S., Chen, S., Lu, X., Hu, S., Wu, J., Chan, C.-K., Chen, S., Zhou, L., Yu, N., Liu, H., Guo, J., Qin, T., Liu, T.-Y.: Target-aware molecule generation for drug design using a chemical language model*. bioRxiv (2024) <https://arxiv.org/abs/https://www.biorxiv.org/content/early/2024/02/01/2024.01.08.574635.full.pdf>. <https://doi.org/10.1101/2024.01.08.574635>
- [49] Guan, J., Qian, W.W., Peng, X., Su, Y., Peng, J., Ma, J.: 3d equivariant diffusion for target-aware molecule generation and affinity prediction. In: The Eleventh International Conference on Learning Representations (2023). <https://openreview.net/forum?id=kJqXEPXMSE0>
- [50] Peng, X., Luo, S., Guan, J., Xie, Q., Peng, J., Ma, J.: Pocket2Mol: Efficient molecular sampling based on 3D protein pockets. In: Chaudhuri, K., Jegelka, S., Song, L., Szepesvari, C., Niu, G., Sabato, S. (eds.) Proceedings of the 39th International Conference on Machine Learning. Proceedings of Machine Learning Research, vol. 162, pp. 17644–17655.

- PMLR, ??? (2022). <https://proceedings.mlr.press/v162/peng22b.html>
- [51] Trott, O., Olson, A.J.: Autodock vina: Improving the speed and accuracy of docking with a new scoring function, efficient optimization, and multithreading. *Journal of Computational Chemistry* **31**(2), 455–461 (2010) <https://arxiv.org/abs/https://onlinelibrary.wiley.com/doi/pdf/10.1002/jcc.21334>. <https://doi.org/10.1002/jcc.21334>
- [52] Eberhardt, J., Santos-Martins, D., Tillack, A.F., Forli, S.: Autodock vina 1.2.0: New docking methods, expanded force field, and python bindings. *Journal of Chemical Information and Modeling* **61**(8), 3891–3898 (2021). <https://doi.org/10.1021/acs.jcim.1c00203>
- [53] Tangallapally, R., Subramanian, C., Yun, M.-K., Edwards, A., Sharma, L.K., Yang, L., Creed, K., Wang, J., Jackowski, S., Rock, C.O., White, S.W., Lee, R.E.: Development of brain penetrant pyridazine pantothenate kinase activators. *Journal of Medicinal Chemistry* **67**(16), 14432–14442 (2024). <https://doi.org/10.1021/acs.jmedchem.4c01211>
- [54] Tarr, J.C., Salovich, J.M., Aichinger, M., Jeon, K., Veerasamy, N., Sensintaffar, J.L., Arnhof, H., Samwer, M., Christov, P.P., Kim, K., Wunberg, T., Schweifer, N., Trapani, F., Arnold, A., Martin, F., Zhao, B., Miriyala, N., Sgubin, D., Fogarty, S., Moore, W.J., Stott, G.M., Olejniczak, E.T., Engelhardt, H., Rudolph, D., Lee, T., McConnell, D.B., Fesik, S.W.: Discovery of a myeloid cell leukemia 1 (mcl-1) inhibitor that demonstrates potent in vivo activities in mouse models of hematological and solid tumors. *Journal of Medicinal Chemistry* **67**(16), 14370–14393 (2024). <https://doi.org/10.1021/acs.jmedchem.4c01188>
- [55] Mammoliti, O., Martina, S., Claes, P., Coti, G., Blanque, R., Jagerschmidt, C., Shoji, K., Borgonovi, M., De Vos, S., Marsais, F., Oste, L., Quinton, E., López-Ramos, M., Amantini, D., Brys, R., Jimenez, J.-M., Galien, R., van der Plas, S.: Discovery of glpg3667, a selective atp competitive tyrosine kinase 2 inhibitor for the treatment of autoimmune diseases. *Journal of Medicinal Chemistry* **67**(11), 8545–8568 (2024). <https://doi.org/10.1021/acs.jmedchem.4c00769>
- [56] Pei, Q., Zhang, W., Zhu, J., Wu, K., Gao, K., Wu, L., Xia, Y., Yan, R.: BioT5: Enriching cross-modal integration in biology with chemical knowledge and natural language associations. In: Bouamor, H., Pino, J., Bali, K. (eds.) *Proceedings of the 2023 Conference on Empirical Methods in Natural Language Processing*, pp. 1102–1123. Association for Computational Linguistics, Singapore (2023). <https://doi.org/10.18653/v1/2023.emnlp-main.70>. <https://aclanthology.org/2023.emnlp-main.70>
- [57] Yang, K., Swanson, K., Jin, W., Coley, C., Eiden, P., Gao, H., Guzman-Perez, A., Hopper, T., Kelley, B., Mathea, M., *et al.*: Analyzing learned

- molecular representations for property prediction. *Journal of chemical information and modeling* **59**(8), 3370–3388 (2019)
- [58] Corey, E.J., Wipke, W.T.: Computer-assisted design of complex organic syntheses: Pathways for molecular synthesis can be devised with a computer and equipment for graphical communication. *Science* **166**(3902), 178–192 (1969)
- [59] Segler, M.H., Preuss, M., Waller, M.P.: Planning chemical syntheses with deep neural networks and symbolic ai. *Nature* **555**(7698), 604–610 (2018)
- [60] Maziarz, K., Liu, G., Misztela, H., Kornev, A., Gaiński, P., Hoefling, H., Fortunato, M., Gupta, R., Segler, M.: Chimera: Accurate retrosynthesis prediction by ensembling models with diverse inductive biases. *arXiv preprint arXiv:2412.05269* (2024)
- [61] Schneider, N., Stiefl, N., Landrum, G.A.: What’s what: The (nearly) definitive guide to reaction role assignment. *Journal of Chemical Information and Modeling* **56**(12), 2336–2346 (2016). <https://doi.org/10.1021/acs.jcim.6b00564>. PMID: 28024398
- [62] Dai, H., Li, C., Coley, C., Dai, B., Song, L.: Retrosynthesis prediction with conditional graph logic network. *Advances in Neural Information Processing Systems* **32** (2019)
- [63] Maziarz, K., Tripp, A., Liu, G., Stanley, M., Xie, S., Gainski, P., Seidl, P., Segler, M.: Re-evaluating retrosynthesis algorithms with syntheseus. *Faraday Discussions* (2024)
- [64] Chen, S., Jung, Y.: Deep retrosynthetic reaction prediction using local reactivity and global attention. *JACS Au* **1**(10), 1612–1620 (2021)
- [65] Zhong, Z., Song, J., Feng, Z., Liu, T., Jia, L., Yao, S., Wu, M., Hou, T., Song, M.: Root-aligned smiles: a tight representation for chemical reaction prediction. *Chemical Science* **13**(31), 9023–9034 (2022). <https://doi.org/10.1039/d2sc02763a>
- [66] Han, Y.e.a.: Retrosynthesis prediction with an iterative string editing model. *nature communications* (2024)
- [67] Mariani, V., Biasini, M., Barbato, A., Schwede, T.: IDDT: a local superposition-free score for comparing protein structures and models using distance difference tests. *Bioinformatics* **29**(21), 2722–2728 (2013)
- [68] Wu, R., Ding, F., Wang, R., Shen, R., Zhang, X., Luo, S., Su, C., Wu, Z., Xie, Q., Berger, B., Ma, J., Peng, J.: High-resolution de novo structure

- prediction from primary sequence. bioRxiv (2022). <https://doi.org/10.1101/2022.07.21.500999>
- [69] He, L., Jin, P., Min, Y., Xie, S., Wu, L., Qin, T., Liang, X., Gao, K., Jiang, Y., Liu, T.-Y.: SFM-Protein: Integrative Co-evolutionary Pre-training for Advanced Protein Sequence Representation. arXiv preprint arXiv:2410.24022 (2024)
- [70] Adolf-Bryfogle, J., Kalyuzhniy, O., Kubitz, M., Weitzner, B.D., Hu, X., Adachi, Y., Schief, W.R., Dunbrack Jr, R.L.: Rosettaantibodydesign (rabd): A general framework for computational antibody design. PLoS computational biology **14**(4), 1006112 (2018)
- [71] Jin, W., Wohlwend, J., Barzilay, R., Jaakkola, T.S.: Iterative refinement graph neural network for antibody sequence-structure co-design. In: International Conference on Learning Representations (2021)
- [72] Jin, W., Barzilay, R., Jaakkola, T.: Antibody-antigen docking and design via hierarchical structure refinement. In: International Conference on Machine Learning, pp. 10217–10227 (2022). PMLR
- [73] Kong, X., Huang, W., Liu, Y.: Conditional antibody design as 3d equivariant graph translation. In: The Eleventh International Conference on Learning Representations (2022)
- [74] Gao, K., Wu, L., Zhu, J., Peng, T., Xia, Y., He, L., Xie, S., Qin, T., Liu, H., He, K., *et al.*: Pre-training antibody language models for antigen-specific computational antibody design. In: Proceedings of the 29th ACM SIGKDD Conference on Knowledge Discovery and Data Mining, pp. 506–517 (2023)
- [75] Chen, X., Zhang, Y., Lu, C., Ma, W., Guan, J., Gong, C., Yang, J., Zhang, H., Zhang, K., Wu, S., Zhou, K., Yang, Y., Liu, Z., Wang, L., Shi, B., Shi, S., Xiao, W.: Protenix - advancing structure prediction through a comprehensive alphafold3 reproduction. bioRxiv (2025). <https://doi.org/10.1101/2025.01.08.631967>
- [76] Meng, E.C., Goddard, T.D., Pettersen, E.F., Couch, G.S., Pearson, Z.J., Morris, J.H., Ferrin, T.E.: Ucsf chimerax: Tools for structure building and analysis. Protein Science **32**(11), 4792 (2023) <https://arxiv.org/abs/https://onlinelibrary.wiley.com/doi/pdf/10.1002/pro.4792>. <https://doi.org/10.1002/pro.4792>
- [77] Yang, H., Hu, C., Zhou, Y., Liu, X., Shi, Y., Li, J., Li, G., Chen, Z., Chen, S., Zeni, C., *et al.*: Mattersim: A deep learning atomistic model across elements, temperatures and pressures. arXiv preprint arXiv:2405.04967 (2024)

- [78] Xie, T., Fu, X., Ganea, O.-E., Barzilay, R., Jaakkola, T.S.: Crystal diffusion variational autoencoder for periodic material generation. In: International Conference on Learning Representations (2022). https://openreview.net/forum?id=03RLpj-tc_
- [79] Zeni, C., Pinsler, R., Zügner, D., Fowler, A., Horton, M., Fu, X., Wang, Z., Shysheya, A., Crabbé, J., Ueda, S., Sordillo, R., Sun, L., Smith, J., Nguyen, B., Schulz, H., Lewis, S., Huang, C.-W., Lu, Z., Zhou, Y., Yang, H., Hao, H., Li, J., Yang, C., Li, W., Tomioka, R., Xie, T.: A generative model for inorganic materials design. *Nature* (2025). <https://doi.org/10.1038/s41586-025-08628-5>
- [80] Miller, B.K., Chen, R.T., Sriram, A., Wood, B.M.: Flowmm: Generating materials with riemannian flow matching. arXiv preprint arXiv:2406.04713 (2024)
- [81] Gruver, N., Sriram, A., Madotto, A., Wilson, A.G., Zitnick, C.L., Ulissi, Z.: Fine-Tuned Language Models Generate Stable Inorganic Materials as Text (2024). <https://arxiv.org/abs/2402.04379>
- [82] Antunes, L.M., Butler, K.T., Grau-Crespo, R.: Crystal structure generation with autoregressive large language modeling. *Nature Communications* **15**(1), 10570 (2024). <https://doi.org/10.1038/s41467-024-54639-7>
- [83] Jain, A., Ong, S.P., Hautier, G., Chen, W., Richards, W.D., Dacek, S., Cholia, S., Gunter, D., Skinner, D., Ceder, G., Persson, K.A.: Commentary: The Materials Project: A materials genome approach to accelerating materials innovation. *APL Materials* **1**(1), 011002 (2013) https://arxiv.org/abs/https://pubs.aip.org/aip/apm/article-pdf/doi/10.1063/1.4812323/13163869/011002_1_online.pdf
<https://doi.org/10.1063/1.4812323>
- [84] Scheidgen, M., Himanen, L., Ladines, A.N., Sikter, D., Nakhæe, M., Fekete, A., Chang, T., Golparvar, A., Márquez, J.A., Brockhauser, S., Brückner, S., Ghiringhelli, L.M., Dietrich, F., Lehmborg, D., Denell, T., Albino, A., Näsström, H., Shabih, S., Dobener, F., Kühbach, M., Mozumder, R., Rudzinski, J.F., Daelman, N., Pizarro, J.M., Kuban, M., Salazar, C., Ondračka, P., Bungartz, H.-J., Draxl, C.: Nomad: A distributed web-based platform for managing materials science research data. *Journal of Open Source Software* **8**(90), 5388 (2023). <https://doi.org/10.21105/joss.05388>
- [85] Saal, J.E., Kirklin, S., Aykol, M., Meredig, B., Wolverton, C.: Materials design and discovery with high-throughput density functional theory: The open quantum materials database (oqmd). *JOM* **65**(11), 1501–1509 (2013). <https://doi.org/10.1007/s11837-013-0755-4>

- [86] Kirklin, S., Saal, J.E., Meredig, B., Thompson, A., Doak, J.W., Aykol, M., Rühl, S., Wolverton, C.: The open quantum materials database (oqmd): assessing the accuracy of dft formation energies. *npj Computational Materials* **1**(1), 15010 (2015). <https://doi.org/10.1038/npjcompumats.2015.10>
- [87] Jiao, R., Huang, W., Lin, P., Han, J., Chen, P., Lu, Y., Liu, Y.: Crystal structure prediction by joint equivariant diffusion. *Advances in Neural Information Processing Systems* **36** (2024)
- [88] Lorenz, R., Bernhart, S.H., Höner zu Siederdisen, C., Tafer, H., Flamm, C., Stadler, P.F., Hofacker, I.L.: Viennarna package 2.0. *Algorithms for Molecular Biology* **6**(1), 26 (2011). <https://doi.org/10.1186/1748-7188-6-26>
- [89] Kalvari, I., Nawrocki, E.P., Ontiveros-Palacios, N., Argasinska, J., Lamkiewicz, K., Marz, M., Griffiths-Jones, S., Toffano-Nioche, C., Gautheret, D., Weinberg, Z., Rivas, E., Eddy, S.R., Finn, R., Bateman, A., Petrov, A.I.: Rfam 14: expanded coverage of metagenomic, viral and microrna families. *Nucleic Acids Research* **49**(D1), 192–200 (2020) <https://arxiv.org/abs/https://academic.oup.com/nar/article-pdf/49/D1/D192/35364695/gkaa1047.pdf>. <https://doi.org/10.1093/nar/gkaa1047>
- [90] Nawrocki, E.P., Eddy, S.R.: Infernal 1.1: 100-fold faster rna homology searches. *Bioinformatics* **29**(22), 2933–2935 (2013) https://arxiv.org/abs/https://academic.oup.com/bioinformatics/article-pdf/29/22/2933/48897722/bioinformatics_29_22_2933.pdf. <https://doi.org/10.1093/bioinformatics/btt509>
- [91] Xu, Y., Zhu, J., Huang, W., Xu, K., Yang, R., Zhang, Q.C., Sun, L.: Prismnet: predicting protein–rna interaction using in vivo rna structural information. *Nucleic Acids Research* **51**(W1), 468–477 (2023)
- [92] Wu, Z., Ramsundar, B., Feinberg, E.N., Gomes, J., Geniesse, C., Pappu, A.S., Leswing, K., Pande, V.: Moleculenet: a benchmark for molecular machine learning. *Chemical Science* **9**, 513–530 (2018). <https://doi.org/10.1039/C7SC02664A>
- [93] Zhu, J., Xia, Y., Wu, L., Xie, S., Zhou, W., Qin, T., Li, H., Liu, T.-Y.: Dual-view molecular pre-training. In: *Proceedings of the 29th ACM SIGKDD Conference on Knowledge Discovery and Data Mining*. KDD '23, pp. 3615–3627. Association for Computing Machinery, New York, NY, USA (2023). <https://doi.org/10.1145/3580305.3599317>
- [94] Xu, M., Zhang, Z., Lu, J., Zhu, Z., Zhang, Y., Chang, M., Liu, R., Tang, J.: Peer: a comprehensive and multi-task benchmark for protein sequence

- understanding. *Advances in Neural Information Processing Systems* **35**, 35156–35173 (2022)
- [95] Dalla-Torre, H., Gonzalez, L., Mendoza-Revilla, J., Carranza, N.L., Grzywaczewski, A.H., Oteri, F., Dallago, C., Trop, E., de Almeida, B.P., Sirelkhatim, H., et al.: The nucleotide transformer: Building and evaluating robust foundation models for human genomics. *BioRxiv*, 2023–01 (2023)
- [96] Zhou, Z., Ji, Y., Li, W., Dutta, P., Davuluri, R., Liu, H.: Dnabert-2: Efficient foundation model and benchmark for multi-species genome. *arXiv preprint arXiv:2306.15006* (2023)
- [97] Rafailov, R., Sharma, A., Mitchell, E., Manning, C.D., Ermon, S., Finn, C.: Direct preference optimization: Your language model is secretly a reward model. *Advances in Neural Information Processing Systems* **36** (2024)
- [98] Mayfield, J., Lowe, D., Sayle, R.: Pistachio: Search and faceting of large reaction databases. In: *ABSTRACTS OF PAPERS OF THE AMERICAN CHEMICAL SOCIETY*, vol. 254 (2017). AMER CHEMICAL SOC 1155 16TH ST, NW, WASHINGTON, DC 20036 USA
- [99] Dunn, A., Wang, Q., Ganose, A., Dopp, D., Jain, A.: Benchmarking materials property prediction methods: The matbench test set and automatminer reference algorithm. *npj Computational Materials* **6**, 138 (2020). <https://doi.org/10.1038/s41524-020-00406-3>
- [100] Xie, T., Wan, Y., Huang, W., Yin, Z., Liu, Y., Wang, S., Linghu, Q., Kit, C., Grazian, C., Zhang, W., et al.: Darwin series: Domain specific large language models for natural science. *arXiv preprint arXiv:2308.13565* (2023)
- [101] Jablonka, K.M., Schwaller, P., Ortega-Guerrero, A., Smit, B.: Is GPT-3 all you need for low-data discovery in chemistry. *ChemRxiv* (2023). <https://doi.org/10.26434/chemrxiv-2023-fw8n4>
- [102] Breuck, P.-P.D., Evans, M.L., Rignanese, G.-M.: Robust model benchmarking and bias-imbalance in data-driven materials science: a case study on MODNet. *Journal of Physics: Condensed Matter* **33**(40), 404002 (2021). <https://doi.org/10.1088/1361-648x/ac1280>
- [103] Wang, A.Y.-T., Kauwe, S.K., Murdock, R.J., Sparks, T.D.: Compositionally restricted attention-based network for materials property predictions. *npj Computational Materials* **7**(1), 77 (2021). <https://doi.org/10.1038/s41524-021-00545-1>

- [104] Eriksson, D., Jankowiak, M.: High-dimensional bayesian optimization with sparse axis-aligned subspaces. arXiv:2103.00349 [cs, stat] (2021) <https://arxiv.org/abs/2103.00349> [cs, stat]
- [105] Dubois, Y., Galambosi, B., Liang, P., Hashimoto, T.B.: Length-controlled alpacaeval: A simple way to debias automatic evaluators. arXiv preprint arXiv:2404.04475 (2024)
- [106] Chen, J.H., Linstead, E., Swamidass, S.J., Wang, D., Baldi, P.: Chemdb update–full-text search and virtual chemical space. *Bioinformatics* **23**(17), 2348–2351 (2007)
- [107] Ye, G., Cai, X., Lai, H., Wang, X., Huang, J., Wang, L., Liu, W., Zeng, X.: Drugassist: A large language model for molecule optimization. arXiv preprint arXiv:2401.10334 (2023)
- [108] Luo, R., Sun, L., Xia, Y., Qin, T., Zhang, S., Poon, H., Liu, T.-Y.: Biogpt: generative pre-trained transformer for biomedical text generation and mining. *Briefings in Bioinformatics* **23**(6), 409 (2022) <https://arxiv.org/abs/https://academic.oup.com/bib/article-pdf/23/6/bbac409/47144271/bbac409.pdf>. <https://doi.org/10.1093/bib/bbac409>

A Supplementary figures

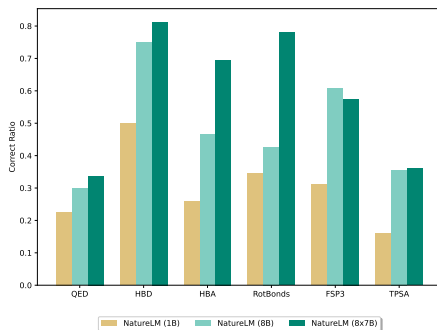


Fig. S1: Correct ratio of property-to-molecule generation. We treat the generated molecule as a correct one if $|v' - v| \leq \delta$, where v' is its property value and v is the input value. Tolerance threshold δ is set to 0 for HBA, HBD, RotBonds, 0.05 for QED and FSP3, and 5 for TPSA.

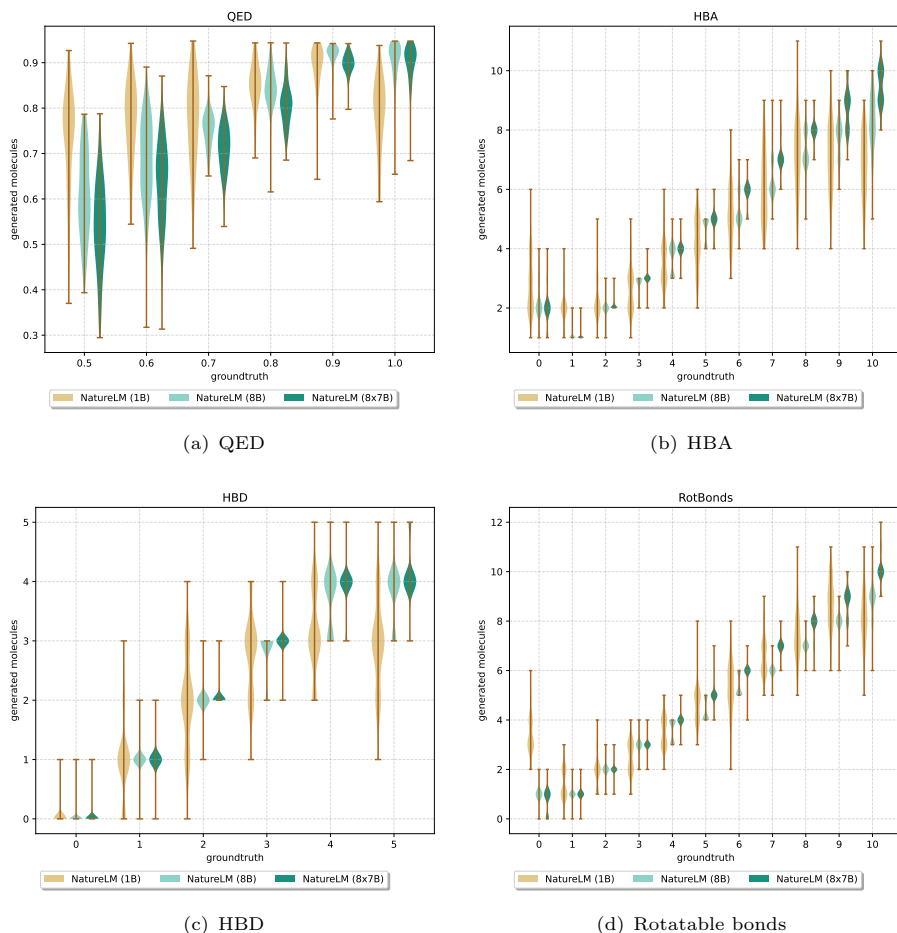


Fig. S2: Violin plot of basic molecular properties for molecule generation, including QED, the number of hydrogen bond acceptors (HBA), the number of hydrogen bond donors (HBD) and the number of rotatable bonds.

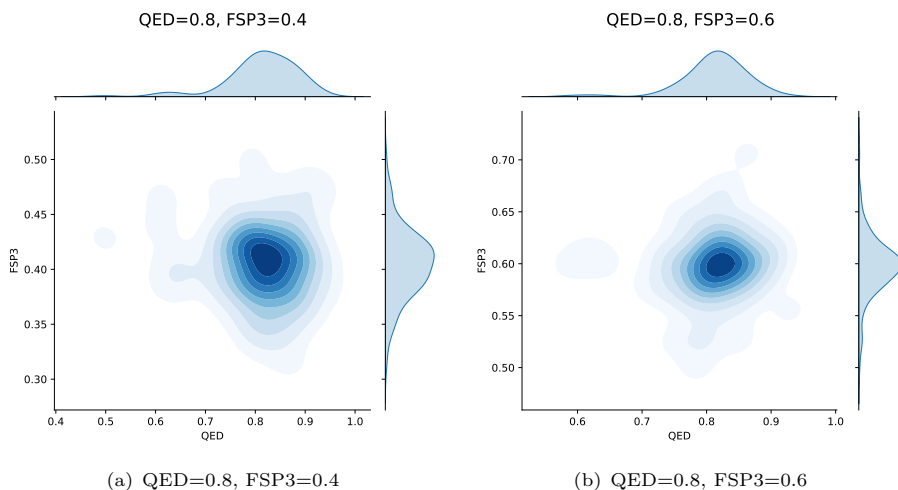


Fig. S3: Heatmap of molecule generation based on QED and fraction of sp^3 (FSP3) properties. Each generated compound's QED and FSP3 values are calculated using RDKit and visualized in the heatmap.

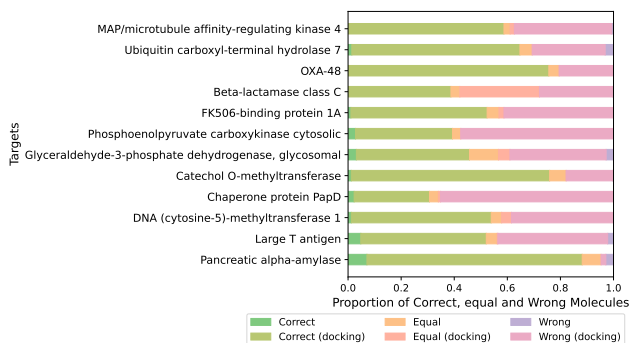


Fig. S4: Bar plot of the proportion of correct, equal and wrong generated molecules. Molecules evaluated by retrieval and molecules evaluated by docking are distinguished using different colors.

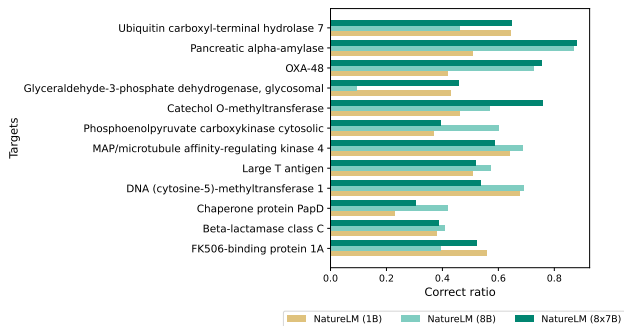


Fig. S5: Bar plot of the correct ratio of NatureLM (1B), NatureLM (8B) and NatureLM (8x7B) on each target.

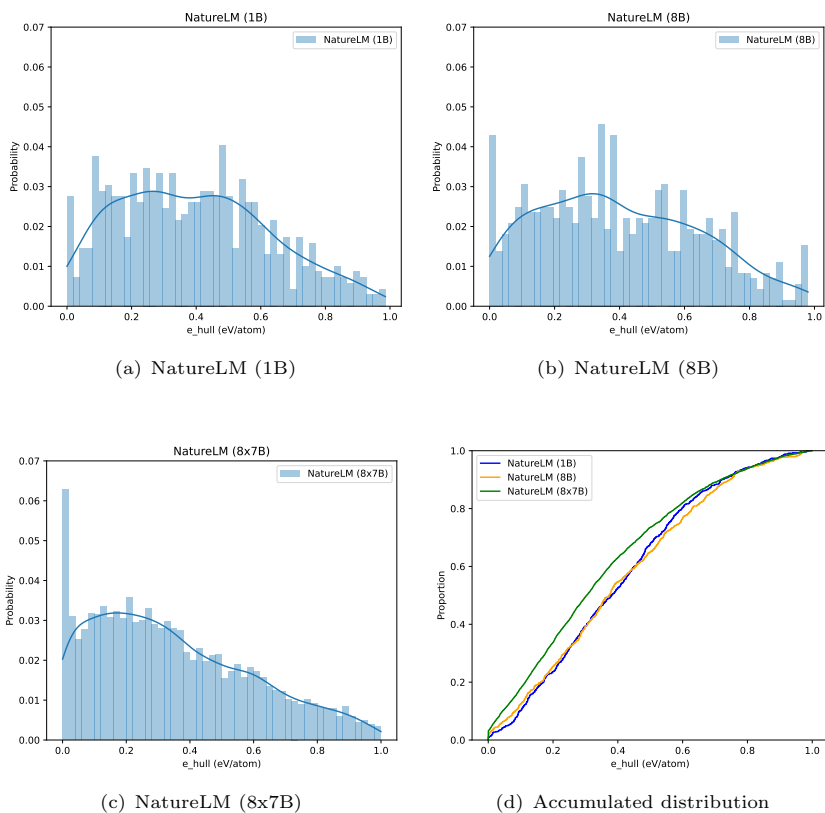


Fig. S6: Energy above hull (ehull) distribution for unconditional material generation.

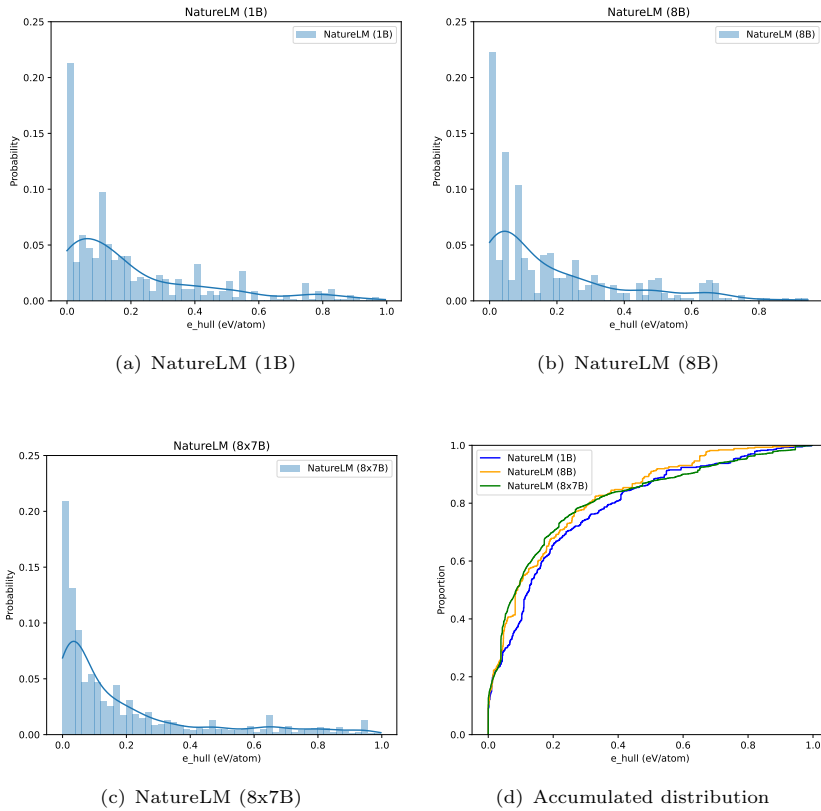


Fig. S7: Energy above hull (ehull) distribution for bulk modulus to material generation.

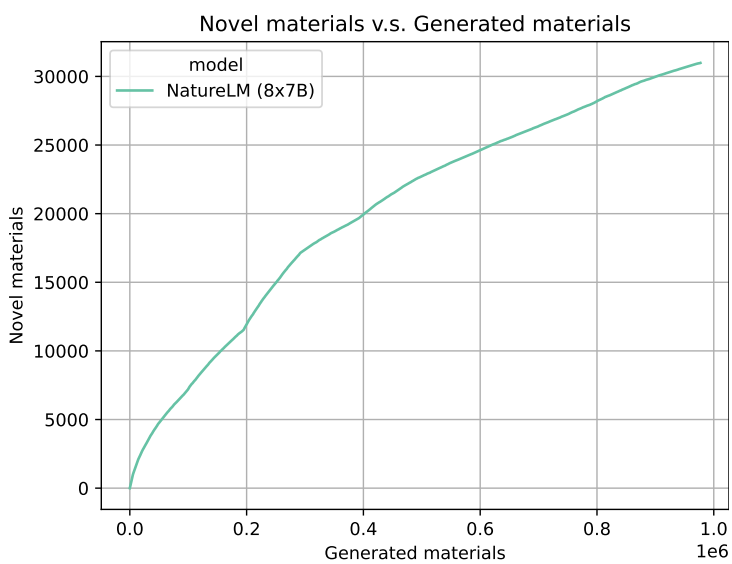


Fig. S8: Novel materials w.r.t generated materials.

Example 1:

PubChem CID: 172655007 (created at February 24, 2025)

SMILES: CC(C)C[C@H]1C(=O)N(Cc2cccc3ccccc23)C[C@@H]2N(C(=O)NCc3ccccc3)CCC(=O)N21

Reference: (6S,9aS)-N-benzyl-6-(2-methylpropyl)-8-(naphthalen-1-ylmethyl)-4,7-dioxo-3,6,9,9a-tetrahydro-2H-pyrazino[1,2-a]pyrimidine-1-carboxamide

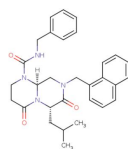
NatureLM: (6S,9aS)-N-benzyl-6-(2-methylpropyl)-8-(naphthalen-1-ylmethyl)-4,7-dioxo-3,6,9,9a-tetrahydro-2H-pyrazino[1,2-a]pyrimidine-1-carboxamide

DeepSeek-R1: (3S,6R)-3-(2-methylpropyl)-6-[(naphthalen-1-yl)methyl]-2,5-dioxo-N-(phenylmethyl)-1,4-diazepancarboxamide

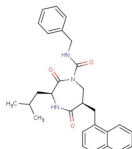
GPT-4o: (3aS,6aR)-N-(benzhydryl)-2,3,3a,4,5,6-hexahydro-1H-pyrrolo[3,4-b]quinolin-5-carboxamide

GPT-4.5: (3S,8aS)-N-Benzyl-3-(benzylcarbamoyl)-hexahydro-2-(2-methylpropyl)-1H-imidazo[1,2-a]pyrazine-1,4(3H,8aH)-dione

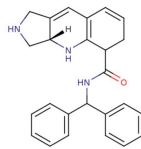
o3-mini: (2S,8R)-8-[(benzylcarbamoylmethyl)amino]-2-[(naphthalen-2-yl)methyl]-4-(1-methylpropyl)-3,6-dioxo-1,4-diazabicyclo[4.3.1]decane



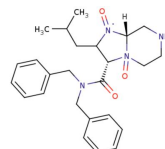
Reference / NatureLM



DeepSeek-R1



GPT-4o



GPT-4.5-preview

Example 2:

PubChem CID: 172655008 (created at February 24, 2025)

SMILES: CC(C)CCN1C(=O)CCN(C(=O)NCc2cccc2)[C@H]1CN(C(=O)Cc1cccc2ccccc12

Reference: (2S)-N-benzyl-2-[[formyl(naphthalen-1-ylmethyl)amino]methyl]-3-(3-methylbutyl)-4-oxo-1,3-diazinane-1-carboxamide

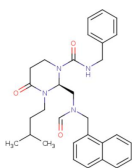
NatureLM: (2S)-N-benzyl-2-[[formyl(naphthalen-1-ylmethyl)amino]methyl]-3-(3-methylbutyl)-4-oxo-1,3-diazinane-1-carboxamide

Deepseek-R1: (3S,6R)-3-(2-methylpropyl)-6-[(naphthalen-1-yl)methyl]-2,5-dioxo-N-(phenylmethyl)-1,4-diazepancarboxamide

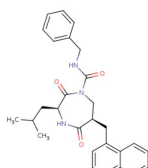
GPT-4o: (3S)-3-[(Benzylamino)carbonyl]-1-(isobutyl)-3,4-dihydro-1H-isoquinolin-2-one

GPT-4.5: (3S)-1-(formylmethyl)-N-(benzylcarbamoyl)-3-(2-methylpropyl)-2-[(naphthalen-1-yl)methyl]piperazine-2,5-dione

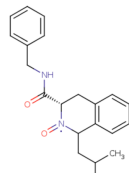
O3-mini: (6S)-N-isobutyl-5-[(benzylcarbamoyl)methyl]-6-[[naphthalen-1-yl)methylcarbamoyl]methyl]-1,5-diazacyclohexan-2-one



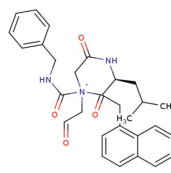
Reference / NatureLM



DeepSeek-R1



GPT-4o



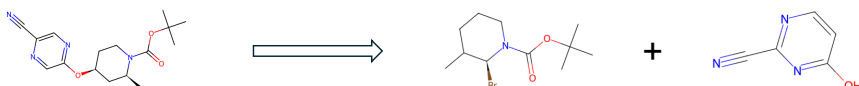
GPT-4.5-preview

Fig. S9: We selected SMILES strings from PubChem with IDs 172655007 and 172655008, which were available as of February 24, 2025, and were excluded from our training set. The performance of NatureLM, DeepSeek-R1 [12], GPT-4o, GPT-4.5-preview, and o3-mini was evaluated for SMILES-to-IUPAC translation. The generated IUPAC names are presented in the accompanying figure. These IUPAC names were subsequently converted back to SMILES for validation. The IUPAC name produced by o3-mini could not be processed due to the high structural complexity of the corresponding molecule. NatureLM successfully generated the correct result. It is important to emphasize that our objective is not to criticize the limitations of general language models but to better understand their current capabilities and explore how they can be complemented by NatureLM for enhanced performance. The molecular structures were visualized using the ChemDB Chemoinformatics Portal [106] <https://cdb.ics.uci.edu/cgi-bin/Smi2DepictWeb.py>.

1) By NatureLM/Reference



2) By DeepSeek-R1



3) By o3-mini-high

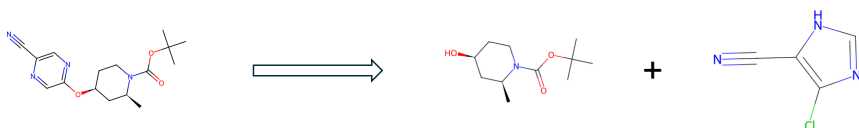
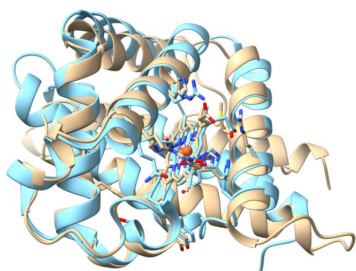
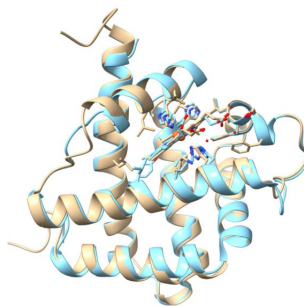


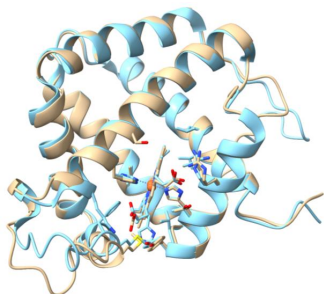
Fig. S10: Additional examples on retrosynthesis prediction. We evaluated the performance of NatureLM, DeepSeek-R1, and o3-mini-high using a reaction from U.S. Patent ID US11999726B2, granted to Eli Lilly on June 04, 2024. The product features two ring systems with a protecting functional group, suggesting that the previous synthesis step likely involved a reaction to connect these rings. Notably, an ether bond links the two rings, with a pyrazine ring on one side and a piperidine ring on the other. Substitution on the pyrazine ring is a common strategy due to its electrophilicity, which often leads to substitution reactions. In this case, NatureLM accurately predicted the cleavage site of the molecule, incorporated a common chlorine atom on the pyrazine ring, and preserved the molecule's stereochemistry, providing a reasonable synthetic strategy. In contrast, both DeepSeek-R1 and o3-mini-high models correctly identified the reactive sites but failed to predict the correct reactants due to poor handling of SMILES representations. For instance, DeepSeek-R1 predicted the pyrazine as pyrimidine, altering the nitrogen atom's position, while o3-mini-high converted the six-membered pyrazine directly into a five-membered imidazole. These errors indicate that these general-purpose language models do not fully understand the relationship between chemical structures and their SMILES representations, hindering their ability to perform accurate reaction predictions.



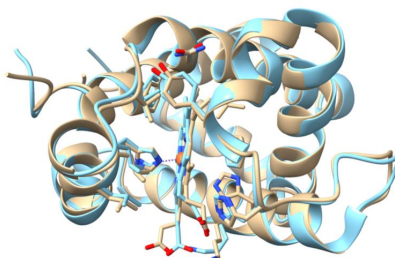
Text description to protein
Reference pdb id = 6Q6P



Text description to protein
Reference pdb id = 1GDJ



SMILES to protein
Reference pdb id = 1D8U



SMILES to protein
Reference pdb id = 1S0H

Fig. S11: Additional examples of designing heme-binding proteins based on text or SMILES instructions are shown. The first two rows display results from the text-based design, while the second row corresponds to the SMILES-based design. The yellow models represent structures generated by NatureLM, whereas the blue models are the reference structures retrieved using the built-in Chimera function. The structures of the generated proteins were predicted using Protenix [75].

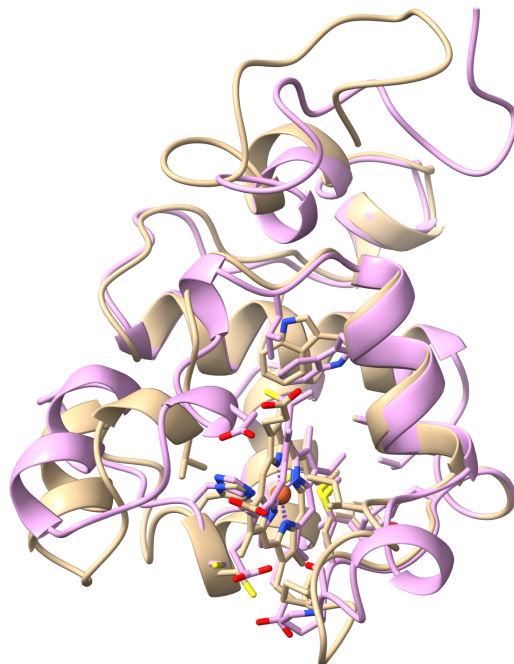


Fig. S12: Comparison of the complex structure of the generated protein with heme (yellow model) and heme C (pink model). The protein was obtained using the SMILES-to-protein approach described in Section 4.5. We observe that they share common structural features. The structures of the generated proteins were predicted using Protenix [75].

For the retrieved PDB structure 3MK7 in Fig. 14, our generated protein aligns to the pocket region that binds to heme C. To further validate this, we used Protenix to predict the binding of our generated protein to both heme C (PubChem CID: 11987638) and heme. The results demonstrate that heme C fits properly into the designed pocket, supporting the structural compatibility of the generated protein with heme C.

This discrepancy arises from the high structural similarity between heme and heme C, as their SMILES representations are nearly identical. Despite this slight misalignment, the output remains biologically relevant because heme-binding proteins often interact with multiple heme derivatives. Furthermore, generating a protein that binds to heme C from the SMILES of heme highlights the algorithm's ability to capture the inherent structural flexibility and functional overlap within the heme family. We will continue improving the algorithm to enhance ligand specificity in future iterations.

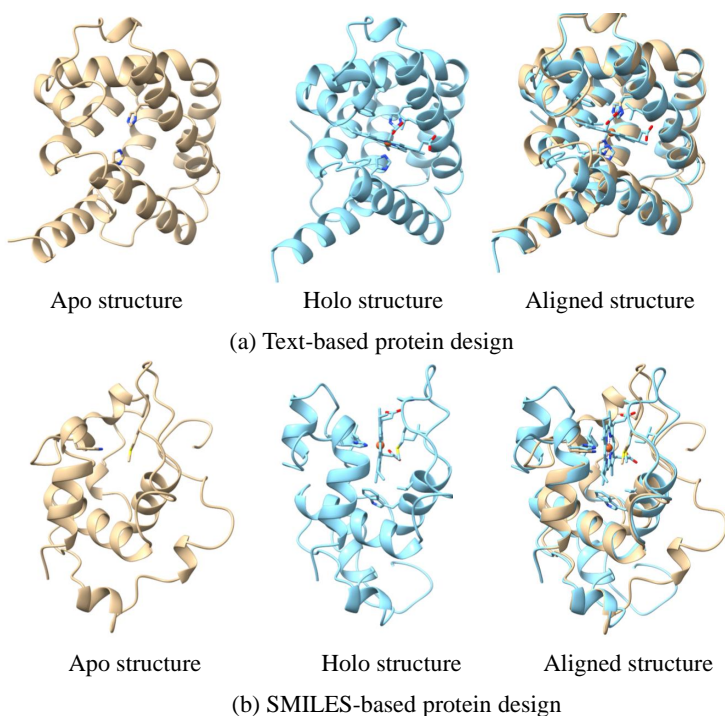


Fig. S13: Comparison of the apo structure of the generated protein, the holo structure in complex with heme, and their aligned structures. Key residues, such as histidine and methionine, occupy similar positions in the pocket region in both the apo and holo structures. This observation suggests that the generated proteins are not only capable of binding heme but also exhibit a structurally pre-formed or conserved binding pocket even in the absence of the ligand. These findings validate the structural plausibility of the designed proteins and their suitability for heme binding.

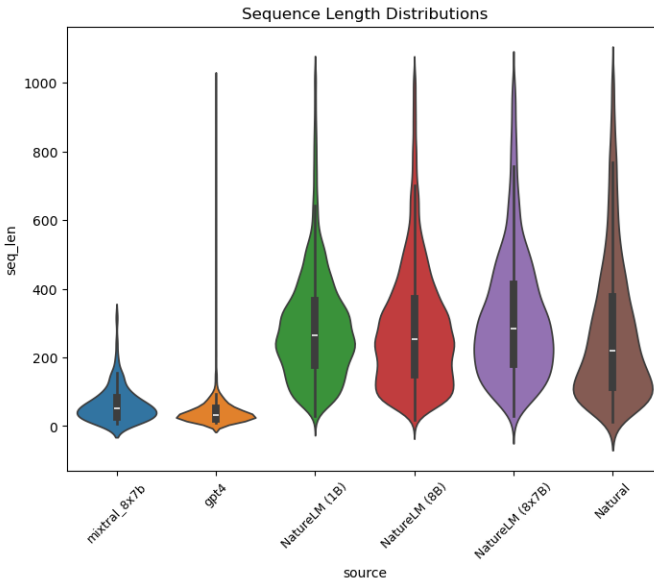


Fig. S14: Sequence length distribution of generated proteins. The NatureLM models demonstrate a more natural distribution that closely resembles the reference UR50 sequences, while Mixtral 8x7B and GPT-4 tend to generate shorter sequences.

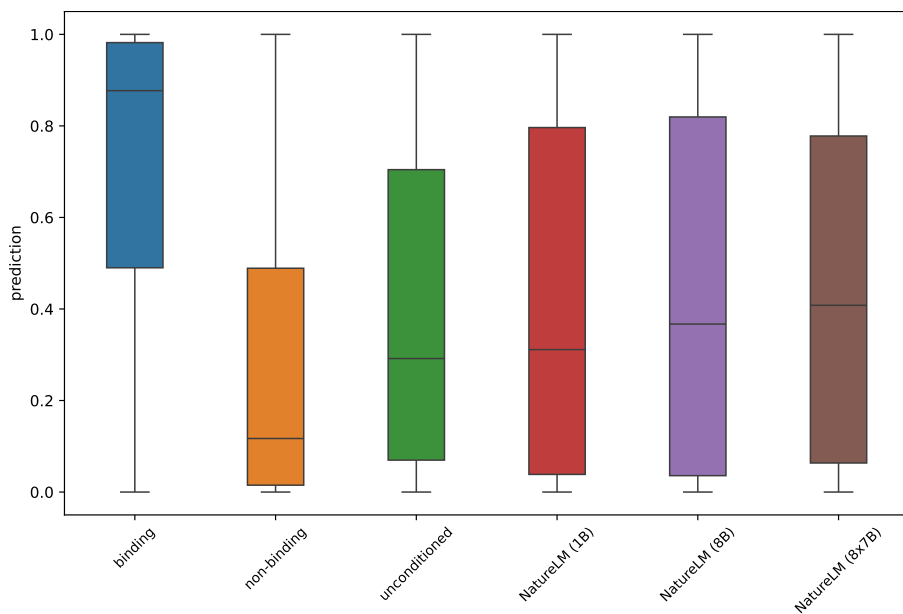


Fig. S15: The distribution of the predicted scores for the RNA sequences in the test set and the generated RNA sequences shows a clear trend. In terms of median values, larger models consistently achieve better predicted scores, indicating stronger binding affinity.

STABLE

- *Please produce a protein sequence that exhibits stability.*
- *I require a stable protein sequence, kindly generate one.*
- *Generate a protein sequence ensuring its stability.*
- *I need a protein sequence that's stable. Please generate it.*
- *Create a stable protein sequence.*
- *Produce a stable protein sequence.*
- *Kindly generate a protein sequence with stability.*
- *I would like you to generate a stable protein sequence.*
- *Please create a protein sequence that ensures stability.*
- *Make a protein sequence that is stable.*

SOLUBLE

- *Generate a soluble protein sequence.*
- *Produce a protein sequence that is soluble.*
- *Create a soluble protein sequence, please.*
- *I require a soluble protein sequence, kindly generate one.*
- *Please produce a protein sequence that exhibits solubility.*
- *Make a protein sequence that is soluble.*
- *Kindly generate a protein sequence with solubility.*
- *I need a protein sequence that's soluble. Please generate it.*
- *I would like you to generate a soluble protein sequence.*
- *Please create a protein sequence that ensures solubility.*

INSOLUBLE

- *Generate an insoluble protein sequence.*
- *Produce a protein sequence that is not soluble.*
- *Create an insoluble protein sequence, please.*
- *I require an insoluble protein sequence, kindly generate one.*
- *Please produce a protein sequence that lacks solubility.*
- *Make a protein sequence that is not soluble.*
- *Kindly generate a protein sequence without solubility.*
- *I need a protein sequence that's insoluble. Please generate it.*
- *I would like you to generate an insoluble protein sequence.*
- *Please create a protein sequence that ensures insolubility.*

Fig. S16: Prompts for conditioned generation

Instruction: *Tell me about Cas9 regarding its cutting mechanism?*

Response:

Cas9 is a CRISPR-associated protein that can be programmed to cut DNA at a specific location. It recognizes a short DNA sequence, called a protospacer, and cuts both strands of the DNA at that site. This DNA cutting is done using two nuclease domains, HNH and RuvC, which are responsible for cutting the top and bottom strands of the DNA, respectively. The HNH nuclease domain cleaves the top strand, while the RuvC nuclease domain cleaves the bottom strand. The cut made by the nuclease domains leaves the DNA with a sticky end that can ligate to another DNA molecule, such as the chromosome of the cell.

Instruction: *Could you provide me the advantages and disadvantages of Cas12a, another widely used CRISPR protein?*

Response:

Advantages:

1. High specificity: Cas12a has higher specificity compared to Cas 9, which reduces off-target effects.
2. Simpler PAM requirements: Cas 12a requires a simpler PAM sequence than Cas9, making it easier to target specific genomic loci.
3. Multiplexing: Cas12a can be used for multiplexing genome editing, meaning multiple genomic loci can be edited in a single reaction.

Disadvantages:

4. Lower efficiency: Cas12a is less efficient in terms of indel formation than Cas9.
5. Larger size: Cas12a is a larger protein than Cas9, which can make it harder to deliver the Cas12a system into cells.
6. Lack of donor specificity: Cas12a has a lower efficiency of HDR than Cas9, which makes it difficult to target specific nucleotides for insertion or deletion.
7. Higher toxicity: Cas12a may cause higher levels of cell death than Cas9, which could impact the overall efficiency of genome editing.
8. Differing DNA repair mechanism: Cas12a and Cas9 utilize different repair mechanisms, which can lead to different outcomes when targeting specific genomic loci.
9. Less versatile: Cas12a is not as versatile as Cas9, as it can only target DNA sequences that contain a TTN PAM sequence.
10. Unclear off-target effects: Cas12a has not been fully characterized in terms of off-target effects, which could lead to unwanted changes in the genome.
11. Difficulty in designing gRNAs: Cas12 requires a longer gRNA sequence compared to Cas9, making it more difficult to design effective gRNAs.

Fig. S17: Response of CRISPR gene editing.

Instruction: *PD-L1, Programmed Death Ligand-1, is a protein that expressed on cancer cells. Design a peptide with 10 amino acids that binds to PD-L1.*

Response: <protein>TDEDVLQKIVKRATEDSSYTVKLSNGQTLVTE
DSEIKKIQKFRS</protein>

Fig. S18: Response of cancer immunotherapy.

Instruction: *Could you explain Lipinski's Rule of Five and its role in evaluating the drug-likeness of chemical compounds?*

Response: Lipinski's Rule of Five, also known as the Rule of Five, is a set of rules developed by Dr. Lipinski that outlines the physical properties of successful orally active drugs. It is a set of simple guidelines that can be used to evaluate the drug-likeness of chemical compounds. It indicates whether a chemical compound with a certain set of properties will have desirable drug-like properties and is likely to be successful as an oral drug. The five rules that comprise Lipinski's Rule of Five are: 1. The number of hydrogen bond donors should be limited to no more than 2. 2. The number of rotatable bonds should be limited to no more than 3. 3. The molecular weight should be less than 500 daltons. 4. The number of hydrogen bond acceptors should be limited to no more than 10. 5. The logD value (a logarithmic measure of a compound's hydrophobicity) should be less than 3. The application of Lipinski's Rule of Five has been widely adopted in the pharmaceutical industry to prioritize lead compounds for drug development. It is a tool that is used to identify potentially promising compounds and can help in the elimination of compounds with poor pharmaceutical properties.

Fig. S19: Response of drug discovery.

Instruction: *How do I wrap a present neatly?*

NatureLM: To wrap a present neatly, start by deciding on the type of wrapping paper you want to use. Next, tear the edges of the paper to make it easier to fold. Wrap the paper around the gift and use tape to hold it in place. Fold the ends of the paper over to form a neat tuck. Finally, tie a bow around the gift to finish it off.

Mixtral: To wrap a present neatly, follow these steps: 1. Gather your supplies: wrapping paper, scissors, tape, and a ruler or measuring tape. 2. Measure the length and width of the present, and cut a piece of wrapping paper that is at least 2 inches longer and wider than the present. 3. Place the present in the center of the wrapping paper, with the bottom of the present facing up. 4. Fold one side of the wrapping paper over the present, and tape it in place. 5. Fold the other side of the wrapping paper over the present, and tape it in place. 6. Fold the top and bottom edges of the wrapping paper over the present, and tape them in place. 7. Flip the present over, and repeat steps 4-6 on the other side. 8. Add a ribbon or bow to the top of the present for a finishing touch.

Instruction: *Write a captivating movie review for a recently released science fiction film, discussing its plot, characters, and special effects.*

NatureLM: It's still quite worth seeing.

Mixtral: Captivating Movie Review: "Interstellar" "Interstellar" is a science fiction film directed by Christopher Nolan, starring Matthew McConaughey, Anne Hathaway, and Jessica Chastain. The film follows a group of astronauts as they travel through a wormhole in search of a new home for humanity. The plot of "Interstellar" is complex and thought-provoking, exploring themes of time, space, and the human condition. The characters are well-developed and relatable, with McConaughey delivering a powerful performance as the lead astronaut, Cooper. The special effects in "Interstellar" are breathtaking, with stunning visuals of space and otherworldly landscapes. The film also features a haunting score by Hans Zimmer, which adds to the emotional impact of the story. Overall, "Interstellar" is a captivating and thought-provoking film that will leave audiences pondering the mysteries of the universe long after the credits roll.

Fig. S20: Response of AlpacaEval.

B Supplementary tables

Data source	Samples (by million)	Tokens (by billion)	Samples (%)	Tokens (%)
Text	46.3	14.4	11.6	10.0
Small molecule	68.0	4.2	17.0	2.9
Protein	192.0	65.2	47.9	45.3
DNA	13.4	19.8	3.3	13.8
RNA	37.8	27.5	9.4	19.1
Material	1.1	0.02	0.3	0.014
Cross-domain	41.9	12.7	10.5	8.8
Total	400.5	143.8	100	100

Table S1: Tokens numbers and their distribution of each domain.

Model Parameters	1B	8B	8x7B
Learning Rate	1e-4	1e-4	2e-4
Batch Size (Sentences)	4096	2048	1536
Context Length (Tokens)	8192	8192	8192
GPU number (H100)	64	256	256

Table S2: Training recipe of different models.

Porperty	Value
QED	0.5, 0.6, 0.7, 0.8, 0.9, 1.0
HBA	0, 1, 2, 3, 4, 5, 6, 7, 8, 9, 10
HBD	0, 1, 2, 3, 4, 5
FSP3	0.0, 0.1, 0.2, 0.3, 0.4, 0.5, 0.6, 0.7, 0.8, 0.9, 1.0
RotBonds	0, 1, 2, 3, 4, 5, 6, 7, 8, 9, 10
TPSA	20, 40, 60, 80, 100, 120

Table S3: Input property values for property-to-molecule generation

Target	Spearman correlation
Pancreatic alpha-amylase	0.569
Large T antigen	0.572
DNA (cytosine-5)-methyltransferase 1	0.517
Chaperone protein PapD	0.739
Catechol O-methyltransferase	0.638
Glyceraldehyde-3-phosphate dehydrogenase, glycosomal	0.503
Phosphoenolpyruvate carboxykinase cytosolic	0.501
FK506-binding protein 1A	0.606
Beta-lactamase class C	0.560
OXA-48	0.680
Ubiquitin carboxyl-terminal hydrolase 7	0.764
MAP/microtubule affinity-regulating kinase 4	0.782

Table S4: Spearman correlation between docking scores and binding affinity on the selected targets for evaluation.

Basic property Enzyme	QED CYP2C9	QED CYP3A4	donor CYP2C9	donor CYP3A4	LogP CYP2C9	LogP CYP3A4	Average
1B	0.352	0.357	0.501	0.497	0.276	0.280	0.377
8B	0.404	0.428	0.548	0.522	0.332	0.340	0.429
8x7B	0.429	0.427	0.515	0.501	0.355	0.347	0.429

Table S5: Joint optimization of metabolism and a basic property.

Property Name	Training samples	Testing samples
BBBP	1272	199
BACE	90677	152
LogP	8491	473
Donor	8526	478
QED	8466	476
CYP1A2	8076	103
CYP2C9	21589	199
CYP2D6	8067	165
CYP3A4	24376	171
Total	179540	2416

Table S6: Statistics of preference data used in RLHF

C Supplementary notes

C.1 Text-guided basic property optimization of small molecule compounds

We focus on optimizing the basic molecular properties in this section. The input of NatureLM includes a text command and a SMILES sequence to be optimized. We evaluate the optimization results of Quantitative Estimation of Drug-likeness (QED), LogP, and the number of hydrogen bond donors. Following DrugAssist [107], we curated a fine-grained procedure. An illustrative example is provided below and the example is from DrugAssist [107]:

Instruction: With a molecule represented by the SMILES string
<mol>CC(N)=[NH+]CC(=O)N1CCC(O)(Cn2cnc3c(cnn3-c3ccc(N4CCC5(CCOCC5)CC4)cc3)c2=O)CC1</mol>, propose adjustments that can increase its QED value by at least 0.1 compared to the pre-optimized value to make it more drug-like.
 Response: <mol>CC(C)(C)OC(=O)N1CCC(c2ncc(-c3ccc(CC[B-](F)(F)F)cc3)cn2)CC1</mol>.

For QED and hydrogen bond donor property optimization, our instructions cover the following scenarios: (i) increase or decrease the property by δ , where both $\delta = 0$ and $\delta > 0$ are considered, aiming to verify the ability of the model; (2) maintain the properties. For LogP, the instruction is to adjust the LogP value from one specified region to another.

Model	QED	#Donor	LogP
LLAMA 3 8B*	0.62 / 0.43	0.75 / 0.43	0.84 / 0.45
NatureLM (1B)	0.58 / 0.57	0.74 / 0.58	0.63 / 0.60
NatureLM (8B)	0.65 / 0.45	0.81 / 0.44	0.80 / 0.42
NatureLM (8x7B)	0.66 / 0.48	0.80 / 0.47	0.80 / 0.47

Table S7: Comparison between the basic property optimization. In each cell, the success rate and uniqueness ratio are reported.

The results are in Table S7. Notably, as the model size of NatureLM increases, there is a marked improvement in performance metrics across all properties. For instance, NatureLM (8B) surpasses NatureLM (1B) in all categories, indicating enhanced comprehension and manipulation of molecular structures and properties as model complexity grows. Despite DrugAssist* achieving the highest scores overall, our results demonstrate that by further increasing the model size and fine-tuning the training process, there is significant potential to outperform this baseline. The trend observed with the NatureLM models

underscores the importance of model scale and suggests that with continued advancements in model architecture and training methodologies, even better optimization outcomes can be achieved. This validates the proficiency of NatureLM in understanding and applying the given instructions to revise molecular properties accordingly.

C.2 Supplementary information of RNA generation

Minimum free energy (MFE) calculation:

```
./ViennaRNA-2.7.0/src/bin/RNAfold -p --MEA ${input_file}
```

Usage of cmscan:

```
cmscan --rfam --cut_ga --nohmmonly --tblout results_tblout --fmt 2 --clanin Rfam/Rfam.clanin Rfam/Rfam.cm ${input_file}
```

C.3 POSCAR files of crystal structures in Fig. 17

VASPStructure of Re3C			
1.000000			
7.1831247561033589	0.0000000000000000	0.0000000000000000	
0.0000000000000000	1.4245311887791383	2.4673932588460490	
0.0000000000000000	-1.4245311887791383	2.4673932588460490	
Re	C		
3	1		
Direct			
0.5000000000000000	0.6666666666666643	0.6666666666666643	Re1
0.8049243600558619	0.3333333333333357	0.3333333333333357	Re2
0.1950756399441381	0.3333333333333357	0.3333333333333357	Re3
0.0000000000000000	0.6666666666666643	0.6666666666666643	C1

VASPStructure of Os3Re			
1.000000			
8.7432980292995008	0.0000000000000000	0.0000000000000000	
0.0000000000000000	1.3846334542329621	2.3982883660601972	
0.0000000000000000	-1.3846334542329621	2.3982883660601972	
Re	Os		
1	3		
Direct			
0.0000000000000000	0.3333333333333355	0.3333333333333355	Re1
0.7492665073023750	0.6666666666666643	0.6666666666666643	Os1
0.2507334926976250	0.6666666666666643	0.6666666666666643	Os2
0.5000000000000000	0.3333333333333355	0.3333333333333355	Os3

C.4 Supplementary information for evaluation metrics

Success Rate for BBBP and CYP Optimization

For BBBP optimization, our goal is to enhance the BBBP ability of the given compounds. These compounds are selected from the test set of the BBBP dataset in MoleculeNet, and initially, none can cross the BBB. For compounds generated by our AI method, we use BioT5 to predict their ability to cross the BBB. If a compound is predicted to cross, the optimization is considered successful.

For CYP optimization, the objective is to decrease the inhibition ability. Our prediction model uses a sigmoid function in the final layer, where 0 indicates

inhibition and 1 indicates no inhibition. For an input molecule A and output molecule B, with predicted values p_a and p_B , if $p_a > p_b$, the optimization is deemed successful.

C.5 Shift the focus from general text to scientific sequences

Although there are certain sequence-based foundation models for scientific tasks, their main focus is on text-based tasks and scientific understanding, instead of scientific discovery, i.e., discovering new molecules, proteins, and material. In Table S8, we compare NatureLM with several sequence models.

Model	BioGPT	MolXPT
Scope	Biomedical literature	Text and SMILES
Core Capabilities	Biomedical natural language processing	SMILES understanding and generation
Representative Tasks	<ul style="list-style-type: none"> • Biomedical relation extraction • Biomedical question answering • Biomedical document classification 	<ul style="list-style-type: none"> • Molecule property prediction • Text-molecule translation
Training Data	<ul style="list-style-type: none"> • Text only • PubMed items before 2021 • 15M paper titles and abstracts 	<ul style="list-style-type: none"> • 67% pure text tokens • 30M paper titles and abstracts from PubMed • 30M SMILES from PubChem • 8M interleaved sequences between SMILES and text
Training Strategy	Trained from scratch	Trained from scratch
Model	Galactica	NatureLM
Scope	Academic literature	Broader "language of nature"
Core Capabilities	<ul style="list-style-type: none"> • Scientific knowledge and reasoning • Scientific writing assistance 	<ul style="list-style-type: none"> • Scientific entity generation • Scientific entity optimization
Representative Tasks	<ul style="list-style-type: none"> • Scientific Q&A • Citation prediction • Equation recall 	<ul style="list-style-type: none"> • Molecule optimization • Protein-to-molecule design • Guide RNA engineering
Training Data	<ul style="list-style-type: none"> • More than 90% pure text tokens • Academic text (e.g., papers, knowledge bases) 	<ul style="list-style-type: none"> • 10% pure text tokens • Diverse scientific sequences (e.g., SMILES, FASTA, DNA, RNA, material, text.)
Training Strategy	Trained from scratch	Continual pre-training on existing LLMs. Incorporates domain-specific instructions

Table S8: Comparison between existing sequence models and NatureLM.

BioGPT [108] and MolXPT [21] are designed for the biomedical and (small) molecular domains. BioGPT is trained with titles and abstracts from PubMed items. MolXPT is trained with PubMed items as well as SMILES from PubChem. Their core capabilities are natural language tasks. Galactica [26] is primarily designed for understanding and reasoning about academic literature. Its core capabilities include recalling equations, answering scientific questions, and performing domain-specific reasoning such as predicting chemical reactions and deriving mathematical proofs. It is trained on a highly curated corpus, primarily consisting of academic texts such as research papers (e.g., arXiv, PMC), reference materials, knowledge bases, LaTeX equations, and structured factual datasets. Notably, **over 90%** of Galactica’s training data consists of pure text, reflecting its emphasis on “academic text” and its key application in scientific writing.

In contrast, NatureLM envisions a broader “language of nature” that unifies multiple scientific domains and modalities. It is explicitly designed to process diverse sequence-based data, including small molecules (SMILES), proteins (FASTA), materials (composition, space group, and atomic coordinates), as well as DNA and RNA sequences. Unlike Galactica, which focuses on understanding and reasoning within scientific text, NatureLM focuses on generative tasks for scientific discovery, especially cross-domain generation and optimization tasks, such as protein-to-molecule design or guide RNA engineering.

Only **10%** training data of NatureLM is pure text. The remaining **90%** consists of scientific entities and cross-domain sequences. Furthermore, NatureLM incorporates cross-domain data where text is interlinked with SMILES, FASTA, and material representations, enabling it to span multiple scientific disciplines through sequence-based formats. This emphasis on structured scientific data allows NatureLM to bridge multiple domains and facilitates discovery-oriented tasks beyond text-based scientific reasoning.